Chemical Geology 472 (2017) 8–21

Contents lists available at ScienceDirect

Chemical Geology

journal homepage: www.elsevier.com/locate/chemgeo

Improved accuracy of LA-ICP-MS U-Pb ages of Cenozoic zircons by alpha dose correction

Sliwinski J.T.[a,*], Guillong M.[a], Liebske C.[a], Dunkl I.[b], von Quadt A.[a], Bachmann O.[a]

[a] ETH Zürich, Institute for Geochemistry & Petrology, Zürich, Switzerland
[b] University of Göttingen, Sedimentology & Environmental Geology, Göttingen, Germany

ARTICLE INFO

Keywords:
Laser ablation ICP-MS
Chemical abrasion
U-Pb zircon geochronology
Matrix effects
Element fractionation

ABSTRACT

While Laser Ablation Inductively-Coupled-Plasma Mass Spectrometry (LA-ICP-MS) is the method of choice for U-Pb dating of zircons in provenance analysis, its application to young (< 100 Ma) zircons is hindered by systematic analytical bias. In magmatic petrology, where the majority of studied units are young, this often places zircon dates at odds with established $^{40}Ar/^{39}Ar$ eruption ages or high-precision ID-TIMS crystallization ages. Zircon lattice properties, particularly the degree of lattice damage caused by the radioactive decay of U and Th, impart analytical bias by causing differential ablation rates and therefore differential fractionation of U and Pb throughout each analysis. Although it is possible to normalize the zircon lattice strengths to calibration reference zircons by thermal annealing to some extent, this may not entirely alleviate the problem. In this study, the effects of alpha decay dose (i.e., degree of radiation damage) on analytical biases in age determination are examined by analyzing a number of zircon reference materials under well-constrained analytical parameters. A regression-based, multi-standard correction method is demonstrated, which improves the accuracy of age data, particularly in young (Cenozoic) zircons. A novel data reduction scheme (Dose_Corrector.ipf) is introduced, which runs in conjunction with the widely-used Igor Pro/Iolite platform and performs a correction for alpha dose and Th disequilibrium. This scheme improves the accuracy of age data for unannealed zircons, and its utility is demonstrated by applying it to zircons from several well-studied units.

1. Introduction

Laser ablation-inductively coupled plasma-mass spectrometry (LA-ICP-MS) is a powerful in situ U-Pb dating technique as it combines high sample throughput with high spatial resolution and analytical uncertainty that approaches that of secondary ion mass spectrometry (SIMS; Simonetti et al., 2005; Gerdes and Zeh, 2006; Guillong et al., 2014; Schaltegger et al., 2015; Guillong et al., 2016). With such precision, it is possible to date zircons in volcanic units as young as Holocene in age, and perhaps even to resolve rates of magmatic processes. However, while $^{206}Pb/^{238}U$ ratios can be measured with a relative precision better than 1% at the 2s level (particularly with multi-collector systems), analytical bias frequently places LA-ICP-MS dates at odds with other age determination methods such as zircon U-Pb isotope dilution thermal ionization mass spectrometry (ID-TIMS; see Mills and Coleman, 2013; Chelle-Michou et al., 2014) and sanidine $^{40}Ar/^{39}Ar$ dating (Zimmerer and McIntosh, 2012; Martiny et al., 2013; Lukács et al., 2015). In total, analytical bias decreases the precision of U-Pb LA-ICP-MS dates to about 2% (Klotzli et al., 2009; Košler et al., 2013), and even when propagated into the total uncertainty, compromises the accuracy of zircon dates and leads to unreliable weighted mean calculations (Horstwood et al., 2016). Given the growing interest in the rates of magmatic processes and the need for large, statistically significant datasets, the development of a method to correct for sources of analytical bias may prove valuable to the community at large (Reid et al., 1997; Schmitt et al., 2003; Vazquez and Reid, 2004; Bachmann et al., 2007; Claiborne et al., 2010; Schoene et al., 2012; Storm et al., 2012; Wotzlaw et al., 2013; Cooper and Kent, 2014; Samperton et al., 2015; Barboni et al., 2016; Buret et al., 2016; Buret et al., 2017; Kaiser et al., 2017; Reid and Vazquez, 2017; Samperton et al., 2017; Schaen et al., 2017). While some sources of analytical bias in LA-ICP-MS U-Pb dating have been historically identified and accounted for, others continue to plague the technique. However, before discussing these, one must first distinguish them from dating inaccuracy unrelated to analytical conditions: daughter isotope disequilibrium and Pb loss.

Very young zircons (< 350 ka) contain the parent/daughter isotope pairs ^{238}U-^{230}Th and ^{235}U-^{231}Pa in a state of secular disequilibrium, which is caused by the preferential partitioning of U over Th and Pa

* Corresponding author.
E-mail address: jakub.sliwinski@erdw.ethz.ch (J.T. Sliwinski).

http://dx.doi.org/10.1016/j.chemgeo.2017.09.014
Received 27 April 2017; Received in revised form 8 September 2017; Accepted 11 September 2017
Available online 19 September 2017

into zircon during crystallization (Schärer, 1984; Sakata et al., 2017). Consequently, most zircons contain U/Pb isotope ratios corresponding to dates younger than the true age by ~80 kyr. While this systematic inaccuracy becomes less significant with increasing zircon age, it is imperative that one corrects for this effect in Pleistocene-Holocene zircons. It is important to note that while Th disequilibrium leads to erroneously young U-Pb ages, this effect is unrelated to analytical bias, and even an ideal system without analytical bias would still produce inaccurate ages.

Pb loss is one of the most commonly cited reason for erroneously young ages and for discordance in zircons (along with age domain mixing, common Pb incorporation and daughter isotope disequilibrium). It involves the loss of radiogenic Pb from a zircon over time and is pronounced in metamict zones (i.e. those with extensive crystal lattice damage due to high alpha particle dose; e.g. Chakoumakos et al., 1987). Many authors experimented over decades to develop a technique that would remove this effect (e.g., Tilton, 1956; Silver and Deutsch, 1963), which culminated in the development of chemical abrasion (CA; Mattinson, 2005). Here, zircons are annealed at elevated temperatures (850–1000 °C) for 48 h (thereby repairing the damaged matrix), after which they are leached with hydrofluoric acid (HF) to remove metamict discordant domains. Since its inception, CA has become a standard technique in ID-TIMS, and has more recently been demonstrated to improve the accuracy and precision of LA-ICP-MS and SIMS U-Pb zircon dates, either by thermal annealing alone (Allen and Campbell, 2012; Solari et al., 2015) or by the entire chemical abrasion procedure (Crowley et al., 2014; von Quadt et al., 2014; Watts et al., 2016).

Meanwhile, laser-induced element fractionation (LIEF) is perhaps the most prevalent source of *analytical bias*, and manifests itself in LA-ICP-MS zircon geochronology in various ways, including the so-called "downhole fractionation." Here, the increase in the $^{206}Pb/^{238}U$ ratio throughout the duration of a single ablation imparts a systematically older age as the laser drills deeper into the zircon. While some claim that this has to do with the higher volatility of Pb relative to U (e.g., Eggins et al., 1998), Allen and Campbell (2012) dispute this by demonstrating that the Pb/U ratio does not change with time (i.e. depth) when analyzing glass reference materials. Instead, U-Pb fractionation is seen as a result of increasing amounts of zircon and baddeleyite (ZrO_2) condensation out of the laser plume, in which U (but not Pb) is compatible (Košler et al., 2005). Regardless of the reason, downhole fractionation correction schemes like the one of Gehrels et al. (2008) and Paton et al. (2010) can effectively correct for downhole fractionation by normalizing the Pb/U ratio within the calibration reference material with a regression, and then applying the same regression to the samples. However, when samples differ in their matrix properties from the calibration reference material, measurements are biased even after correction. A sample that ablates slower or faster than the calibration reference material will have a respectively younger or older apparent age (Marillo-Sialer et al., 2014; Marillo-Sialer et al., 2016).

Significant differences in ablation rates between commonly-used reference materials have been demonstrated to result in age offset relative to accepted ID-TIMS ages (Marillo-Sialer et al., 2014). These results were followed by an investigation of "matrix effects," i.e., the role that certain factors play in the ablation of a material. These include: degree of metamictization, crystallographic orientation, crystal color/opacity, application of thermal annealing and concentration of various trace elements (P, Y, Rare Earth Elements (REE); Marillo-Sialer et al., 2016). By far the most important factors were the degree of metamictization and whether or not thermal annealing was applied, which is consistent with work demonstrating that the degree of offset from accepted ID-TIMS ages is proportional to the amount of alpha radiation experienced by a zircon from the decay of U and Th (Allen and Campbell, 2012).

The release of alpha particles during the decay of radioactive nuclides damages the host crystal lattice and its integrity, leading to faster laser ablation rates. The amount of alpha particle dose accumulated by a zircon is therefore a function of the concentrations of U and Th, the age of the zircon and the amount of alpha particle-releasing events in the decay chains of ^{238}U, ^{235}U and ^{232}Th (8, 7 and 6, respectively). In particular:

$$D_\alpha = 8^*\frac{c_U{}^*N_A{}^*0.9928}{M_{238}{}^*10^6}{}^*(e^{\lambda_{238}t} - 1) + 7^*\frac{c_U{}^*N_A{}^*0.0072}{M_{235}{}^*10^6}{}^*(e^{\lambda_{235}t} - 1) + 6^*\frac{c_{Th}{}^*N_A}{M_{232}{}^*10^6}{}^*(e^{\lambda_{232}t} - 1) \quad (1)$$

where D_α represents the alpha dose (events per g), c_U and c_{Th} represent the concentration of U and Th in $\mu g\ g^{-1}$ (respectively), N_A represents Avogadro's number, M_{232}, M_{235} and M_{238} represent the molecular masses of ^{232}Th, ^{235}U and ^{238}U, and λ_{232}, λ_{235} and λ_{238} represent their respective decay constants (s^{-1}) (Jaffey et al., 1971; Steiger and Jäger, 1977; Mattinson, 2010).

However, natural thermal annealing in the form of metamorphism and thermal events in the history of a zircon may repair the crystal lattice, in which case the amount of analytical bias will be less than the total alpha dose would suggest (Marillo-Sialer et al., 2016). It is partly for this reason that Allen and Campbell (2012) and Marillo-Sialer et al. (2016) suggested to apply thermal annealing, thereby ensuring relatively similar thermal histories for all zircons. Because this is not always possible (e.g. in thin sections), one must find a way to reliably correct for alpha dose-related analytical bias. The thermal histories of young zircons are typically easier to constrain due to limited time available for metamorphism and exhumation, thereby facilitating such an approach. It is in these zircons that the largest analytical biases are observed, and where the disagreement between LA-ICP-MS U-Pb ages and $^{40}Ar/^{39}Ar$ ages is the most prominent (Zimmerer and McIntosh, 2012; Lukács et al., 2015).

The goal of the present study is to introduce an offline empirical correction scheme for LA-ICP-MS zircon U-Pb datasets by modeling a regression curve through age offset and alpha dose data and propagating the uncertainty on the regression to the final age. An alternate method of estimating analytical uncertainty based on several validation reference materials is also presented, which forgoes error propagation in lieu of an empirical approach. A new data reduction scheme is developed (Dose_Corrector.ipf), which is validated on multiple zircon reference materials and leads to a decrease in systematic age bias and improved reproducibility. This approach is tested using an identical analytical setup in two different laboratories (ETH Zürich and University of Göttingen). Additionally, the method is tested on zircons from units which have well-characterized sanidine $^{40}Ar/^{39}Ar$ eruption ages and/or high-precision ID-TIMS zircons ages that can serve as quality control for LA-ICP-MS data: the 28.02 Ma Fish Canyon Tuff (Phillips and Matchan, 2013; Wotzlaw et al., 2013), the ~11 Ma La Gloria Pluton (Gutierrez et al., 2013; Payacán et al., 2014) and the 26.91 Ma Rat Creek Dacite (Lipman and McIntosh, 2008). Finally, it is proposed that while thermal annealing aids in the acquisition of accurate age data, it is optional in light of the new data correction scheme.

2. Methods

2.1. Reference materials

In order to assess the degrees of analytical bias among zircon U-Pb ages by LA-ICP-MS, we selected a number of zircon reference materials with well-constrained ID-TIMS ages. In order to verify the linear relationship between analytical bias and log of alpha dose, and to extend this relationship to younger samples, we developed a calibration curve based on reference materials of variable age and alpha dose (Fig. 1). We used GJ-1 (601.86 ± 0.37 Ma; Jackson et al., 2004; Horstwood et al., 2016) as a calibration reference zircon, and a host of validation reference zircons, listed in Table 1.

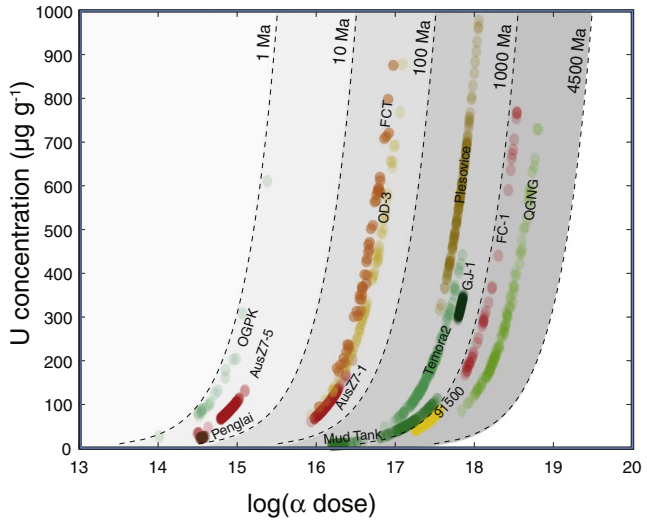

Fig. 1. α radiation dose vs U concentration (μg g^{-1}) for reference zircons in this study. Contours represent time used in calculation (Ma). Reference materials in the present study cover the age range of 1–1842 Ma and log(α dose) range from ~14–18.5.

Reference zircons were split into two groups: (1) chemically abraded and (2) untreated. Chemically abraded zircons were prepared according to procedures laid out by Mattinson (2005): zircons were thermally annealed at 850 °C for 48 h in quartz crucibles, after which they were enclosed in 3 ml Savillex vials with 48% HF. The vials were heated in Parr vessels at 140 °C for 14 h, after which the zircons were washed in deionized water (four times) and distilled acetone (four times). Then, the zircons were left in 6 N double-distilled HCl overnight at ~70 °C, after which the washing procedure with water and acetone was repeated. The abraded zircons were then mounted in epoxy and polished with SiC paper and diamond paste to a finish of < 1 μm.

2.2. LA-ICP-MS instrumentation and data reduction

Data were collected over the course of fourteen months at ETH Zürich using an ASI Resolution 193 nm ArF excimer laser equipped with a Laurin Technic 155 constant geometry 2-volume ablation cell connected to a Thermo Element XR sector field ICP-MS. Ablation took place under pure He atmosphere (0.7 l/min), which was mixed with Ar within the funnel. The ablated material was homogenized using a signal smoothing device prior to entry into the ICP. In order to test the viability of our data correction method, we collected data at the University of Göttingen (GÖ) in addition to ETH Zürich. The instrumental setup at GÖ is identical to ETHZ's, and the analytical parameters are therefore similar. More information can be found in Table 2, where minor differences in procedure are listed. It should be noted that differences in acquisition properties do not affect the results, as the alpha-dose calibration is calculated separately for every analytical session.

Data at ETH were reduced using the VizualAge data reduction scheme (DRS; Petrus and Kamber, 2012) running Iolite v2.5 (Paton et al., 2011). The reduction scheme includes (in brief): baseline subtraction of raw counts of Hg, Pb, U and Th isotopes (masses 202, 204, 206, 207, 208, 232 and 238), calculation of ratios, instrumental drift correction, followed by a downhole fractionation correction on the calibration reference material following the scheme of Paton et al. (2010) before final normalization to ID-TIMS U/Pb. Excess uncertainty in the isotopic ratios is calculated by a "pseudosecondary standard" method, whereby individual calibration reference analyses are sequentially removed from the $^{206}Pb/^{238}U$ drift correction spline, and the total variation among all the resultant splines is quadratically added as "excess" uncertainty (Paton et al., 2010). For alpha dose calculation, the U and Th concentrations are approximated by using U and Th counts in the calibration reference material and its known, (importantly, homogeneous) U and Th concentration. Alternatively, one may treat raw counts of ^{206}Pb, ^{207}Pb and ^{208}Pb as proxies for radiation damage in lieu of log(dose) when heterogeneous reference materials (e.g. Temora) are used (Matthews and Guest, 2017).

2.3. Dose corrector

Dose_Corrector.ipf is a new add-on that runs in Iolite on the Igor Pro platform and carries out an empirical correction for alpha dose using a host of validation reference materials. In brief, the program carries out the following calculations: (1) total alpha dose in g^{-1}; (2) for reference materials, the ratio of the measured $^{206}Pb/^{238}U$ age to the reference ID-TIMS age (uncorrected for Th disequilibrium); (3) the regression of log (α dose) vs age offset with 95% confidence intervals; (4) division of all ages by the offset estimated in the regression model; (5) correction for Th disequilibrium; and (6) propagation of errors on the $^{206}Pb/^{238}U$ ratio, alpha dose correction and Th disequilibrium correction. The alpha dose is calculated using measured ages and U and Th concentrations for simplicity. While there are some degrees of uncertainty associated with these parameters, they have little influence on the correction scheme, as it is the log of the dose that is used for regression purposes. Two different regression models are available to the user: either a linear regression or a nonlinear model. In the former case, the 95% confidence bands are used to determine the regression-related uncertainty, and this uncertainty is propagated into each individual date. In the latter case, the uncertainty is determined by the prediction bands of the regression, and no propagation is involved. This is discussed in more detail later (see "Propagation of uncertainty from alpha dose correction").

The user may run Dose_Corrector using either default iolite output .txt files or by manually defining the necessary input parameters from a .txt or .csv file (see Appendix 1,2). These parameters include the final $^{206}Pb/^{238}U$ ratio, final age, propagated 2 s error (corrected for drift, downhole fractionation and normalized to the primary reference value) and U and Th concentrations. The Th disequilibrium correction is performed using the algorithm of Schärer (1984), assuming a constant Th/U partition coefficient ratio of 0.33 ± 0.063 (1σ) (Rubatto and Hermann, 2007). An output table is generated, which includes the Th-corrected ages, the alpha dose-corrected ages and all respective propagated uncertainties.

3. Results

LA-ICP-MS data were collected over 15 measurement sessions between May 2016 and July 2017 (Table 3) and in all cases show good correlations between alpha dose and analytical bias (average $R^2 = 0.84$; Fig. 2). Zircons that were not chemically abraded demonstrated consistently younger ages with decreasing alpha dose, with the youngest zircons (e.g. AusZ7–5; 2.3202 Ma) only measuring 92–96% of their true $^{206}Pb/^{238}U$ ratios. AusZ7–1 (~38.9 Ma) was typically 2–4% too young, while the rest of the reference zircons were, for the most part, within 2% of their reference ID-TIMS values (albeit with a systematic shift toward older ages with higher alpha dose). Comparison of ETH and GÖ (unannealed) data demonstrates a consistent pattern in matrix-related analytical bias between the two labs (Fig. 3). Chemically abraded zircons showed considerably less scatter, and in almost all cases (including the youngest samples) were within 2% of their reference values. It should, however, be noted that even though a large amount of offset was corrected by the chemical abrasion procedure, some bias remained at low alpha dose (average $R^2 = 0.51$; Fig. 2).

While the regression parameters were similar between sessions, there was still some variation which is not readily explainable (Figs. 2–4). Based on limited exploration in this study, there is no obvious trend between laser energy density and regression slope, but it is certainly possible that such complex trends do exist. On one occasion

Table 1
Zircon reference materials used in the current study.

Sample	Age ± 2s (Ma)	Reference	U (μg g^{-1})	1s	log(D_α)[b]	1s	n
Unannealed (ETHZ)							
AusZ7-1	~38.9	Kennedy et al., 2014	101.5	22.4	16.13	0.09	197
AusZ7-5	2.4082 ± 0.0022	von Quadt et al., 2016	85.2	15.8	14.88	0.10	135
FC-1[c]	1099.9 ± 0.6	Paces and Miller, 1993	363.7	211.0	18.16	0.23	39
GJ-1[a]	601.86 ± 0.37	Jackson et al., 2004	321.5	8.4	17.83	0.01	282
Mud Tank[a]	731.65 ± 0.49	Black and Gulson, 1978	59.7	21.5	17.21	0.17	90
Mud Tank[a]	731.65 ± 0.49	Black and Gulson, 1978	9.0	5.7	16.35	0.17	72
OD-3	33.0 ± 0.1	Iwano et al., 2013	389.9	497.2	16.62	0.28	83
OGPK[d]	1.00 ± 0.08	Sakata et al., 2014	147.3	124.2	14.73	0.23	20
Penglai	4.393 ± 0.041	Li et al., 2010	22.6	0.9	14.57	0.02	20
Plešovice[a]	337.16 ± 0.11	Sláma et al., 2008	595.0	149.2	17.83	0.10	152
QGNG	1842.0 ± 3.1	Black et al., 2003b	297.6	184.1	18.35	0.23	109
Temora2	416.78 ± 0.33	Black et al., 2004	187.4	103.7	17.42	0.20	148
91500[a]	1063.51 ± 0.39	Wiedenbeck et al., 1995	68.0	11.6	17.44	0.08	189
Annealed (ETHZ)							
AusZ7-1	~38.9	Kennedy et al., 2014	108.8	11.9	16.17	0.04	50
AusZ7-5	2.4082 ± 0.0022	von Quadt et al., 2016	95.3	14.0	14.92	0.08	47
FC-1[c]	1099.9 ± 0.6	Paces and Miller, 1993	318.0	128.6	18.12	0.16	44
GJ-1[a]	601.86 ± 0.37	Jackson et al., 2004	321.1	6.1	17.83	0.01	117
Mud Tank[a]	731.65 ± 0.49	Black and Gulson, 1978	14.6	0.4	16.60	0.01	50
OD-3	33.0 ± 0.1	Iwano et al., 2013	365.3	186.1	16.62	0.26	34
Plešovice[a]	337.16 ± 0.11	Sláma et al., 2008	593.6	106.9	17.83	0.08	44
QGNG	1842.0 ± 3.1	Black et al., 2003b	266.9	169.3	18.28	0.25	47
Temora2	416.78 ± 0.33	Black et al., 2004	130.4	54.8	17.26	0.18	59
91500[a]	1063.51 ± 0.39	Wiedenbeck et al., 1995	63.6	8.0	17.41	0.06	45
Unannealed (GÖ)							
91500[a]	1063.51 ± 0.39	Wiedenbeck et al., 1995	77	14	17.49	0.01	66
AusZ2	38.8963 ± 0.0044	Kennedy et al., 2014	229	13	16.50	0.03	45
AusZ5	38.9022 ± 0.0035	Kennedy et al., 2014	258	64	16.57	0.01	122
AusZ7-1	~38.89	Kennedy et al., 2014	112	13	16.16	0.03	44
DX-11	240.5 ± 0.5	Pálfy et al., 2003	206	122	17.26	0.11	22
DX-46	14.408 ± 0.018	Lukács et al., 2015	736	261	16.56	0.09	120
FC-1[c]	1099.5 ± 0.5	Paces and Miller, 1993	559	262	18.30	0.31	87
FCT	28.642 ± 0.025	Wotzlaw et al., 2013	352	104	16.53	0.05	45
GJ-1[a]	601.86 ± 0.37	Jackson et al., 2004	295	14	17.79	0.01	211
Mud Tank[a]	731.65 ± 0.49	Black and Gulson, 1978	22	5	16.70	0.10	60
OD-3	33.0 ± 0.1	Iwano et al., 2013	432	197	16.74	0.12	65
OG-1	3440.7 ± 3.2	Stern et al., 2009	144	38	18.46	0.10	20
Plešovice[a]	337.16 ± 0.11	Sláma et al., 2008	645	122	17.87	0.03	127
R33	419.3 ± 0.4	Black et al., 2004	202	93	17.47	0.21	45
Temora2	416.78 ± 0.33	Black et al., 2004	141	46	17.39	0.04	48

[a] Latest age from Horstwood et al., 2016.
[b] D_α represents the alpha particle dose in g^{-1}.
[c] Latest age from Mattinson, 2010.
[d] Fission track age.

(30 Nov 2016), the ^{235}U signal was used to calculate ^{238}U concentration due to poor intercalibration between high and low signals in analog and pulse counting modes, resulting in a shallower regression with larger uncertainties on individual analyses. It is important to note that while deviations such as these may occur, they are still correctable because the biases are internally consistent within the analytical session. The overall pattern of the corrected data demonstrates a marked improvement in age accuracy after alpha dose correction, particularly among the youngest reference materials (Fig. 4).

The external validity of this approach is tested on zircons from several independently-dated units as well as reference materials (Tables 4, 5, Appendix 3). LA-ICP-MS zircon data from the Fish Canyon Tuff yield a weighted mean age of 27.84 ± 0.18 Ma prior to dose correction (Fig. 5), noticeably younger than the weighted mean of ID-TIMS ages of 28.427 ± 0.036 Ma (Wotzlaw et al., 2013) and with the youngest zircons significantly younger than the ^{40}Ar/^{39}Ar eruption age and youngest ID-TIMS ages (~28.2 Ma). Dose correction and Th-disequilibrium correction yields an adjusted weighted mean age of 28.39 ± 0.18 Ma, which is in agreement with ID-TIMS data and the ^{40}Ar/^{39}Ar eruption age (between 27.9 and 28.3 Ma; see Renne et al., 1998; Kuiper et al., 2008; Channell et al., 2010; Renne et al., 2010; Rivera et al., 2011; Westerhold et al., 2012; Phillips and Matchan, 2013). Similarly, the youngest zircons from the Rat Creek Tuff are in agreement with ^{40}Ar/^{39}Ar eruption age at 26.91 Ma. Data from the younger La Gloria Pluton show similar behavior: the youngest dose-corrected zircons from La Gloria overlap with ID-TIMS ages (weighted mean of 5 zircons = 11.2427 ± 0.024 Ma; Szymanowski, unpublished data).

4. Discussion

The cost effectiveness, rapidity and precision (similar to SIMS in applications such as trace element analysis and U-Th dating; Guillong et al., 2016) makes it a first-choice tool in certain applications (e.g. detrital zircon dating). However, analytical bias ultimately limits its application in U-Pb dating (Klotzli et al., 2009). While early work has attributed this to differences in volatility of elements (Longerich et al., 1996; Eggins et al., 1998; Horn and von Blanckenburg, 2007), more recent studies have also attributed this more generally to “matrix effects.” In short, differences in material properties impart variations in

Table 2
Analytical conditions at ETH and Göttingen [GÖ, *italics*].

Laboratory & sample preparation	
Laboratory name	Dept. of Earth Science, ETH Zurich [*GÖ: University of Göttingen*]
Sample type/mineral	Zircon
Sample preparation	Conventional mineral separation, 1-in resin mount, 1 μm polish
Laser ablation system	
Make, model & type	ASI Resolution
Ablation cell & volume	Laurin Technic 155, constant geometry, aerosol dispersion volume < 1 cm^3
Laser wavelength	193 nm
Pulse width	25 ns
Energy density/fluence	2.0–5.5 J cm^{-2}
Repetition rate	4–5 Hz [*GÖ: 5 Hz*]
Spot size	19–29 μm [*GÖ: 33 μm*]
Ablation rate	~75 nm $pulse^{-1}$
Sampling mode/pattern	Single hole drilling, 3 cleaning pulses
Carrier gas and flow	100% He, 0.7 l/min
Ablation duration	40 s [*GÖ: 20 s*]
ICP-MS instrument	
Make, model & type	Thermo Element XR SF-ICP-MS
Sample introduction	Ablation aerosol only, squid-like aerosol homogenization device
RF power	1550 W [*GÖ: 1250 W*]
Make-up gas flow	~0.95 l/min Ar (gas mixed to He carrier inside ablation cell funnel)
Detection system	Single detector triple mode SEM, analogue, Faraday
Masses measured	202, 204, 206, 207, 208, 232, 235, 238 amu
Integration time per peak (mass)	10 ms (202, 204, 208, 232, 235), 20 ms (238), 75 ms (206, 207); [*GÖ: 15 ms (202,204, 232, 234, 238), 30 ms (208), 60 ms (206), 100 ms (207)*]
Integration time per reading	0.25 s
Dead time	20 ns
Typical oxide rate (ThO/Th)	0.18%
Typical (++) rate (Ba^{++}/Ba^{+})	3.50%
Data processing	
Gas blank	30 s prior to each ablation spot
Calibration strategy	GJ-1 used as calibration ref. material; bracketing 2 per 20 samples
Reference material information	601.86 ± 0.37 Ma; U = 312 and Th = 10.8 ppm; Horstwood et al., 2016
Data processing package used	Iolite v2.5 using VizualAge [*GÖ: UranOS v2.08*]
Mass discrimination	Mass bias correction for all ratios normalized to calibration reference material
Uncertainty level & propagation	Ages are quoted at 2s absolute. Propagation is by quadratic addition.

Table 3
Analytical conditions and standard reference materials used by date.

Date	Size (μm)	E (J cm^{-2})	CA[a]	GJ-1	91500	Temora2	Plešovice	AusZ7-1	AusZ7-5	MT(L)[b]	MT(D)[b]	OD-3	FC-1	QGNG	Penglai	OGPK
160527	29	2.0		x	x	x	x	x				x		x		
160529	29	2.5		x	x	x	x	x	x			x		x		
160530	29	2.0		x	x	x	x	x	x			x		x		
160604	29	2.0		x	x	x	x	x	x	x	x	x	x	x	x	x
160608	29	4.0		x	x	x	x	x	x	x	x	x	x	x		
160616	29	2.0	x	x	x	x	x	x	x	x			x	x		
160617	29	2.0	x	x	x	x	x	x	x	x		x	x	x		
160620	29	2.0	x	x	x	x	x	x	x	x		x	x	x		
160711	29	5.5		x	x	x	x	x	x							
160731	29	2.5		x	x	x	x	x								
161010	19	2.5		x	x	x	x	x	x	x	x					
161016	19	2.5		x	x	x	x	x	x		x			x		
161130	29	2.5		x	x	x	x	x	x					x		
161130	29	2.5	x	x	x	x	x	x	x					x		
161211	19	2.5		x	x	x	x	x	x		x	x		x		
170713	29	2.5		x	x	x		x	x							

[a] Chemically abraded.
[b] MT(L) = Mud Tank (light); MT(D) = Mud Tank (dark).

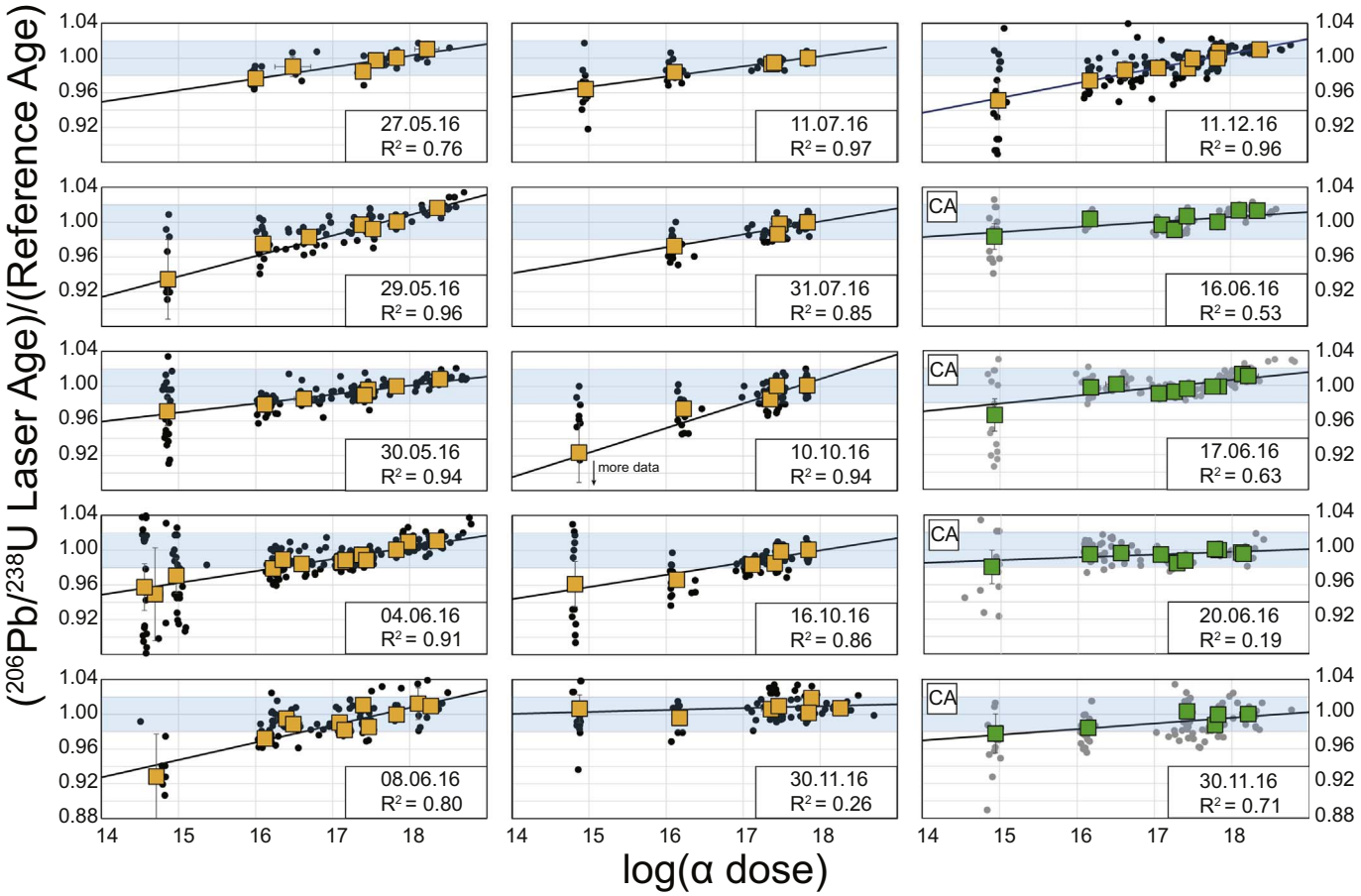

Fig. 2. Age offset (LA-ICP-MS $^{206}Pb/^{238}U$ Age divided by ID-TIMS reference age, both uncorrected for Th-disequilibrium) vs log(dose) for chemically abraded (CA) and non-abraded zircons. Each subplot represents all analyses from one session (black circles) and averages for each reference material (squares). Blue boxes represent ± 2% age offset and error bars represent ± 2 SE (standard error of the mean; typically smaller than symbol). Not shown is data from 13 July 2017.

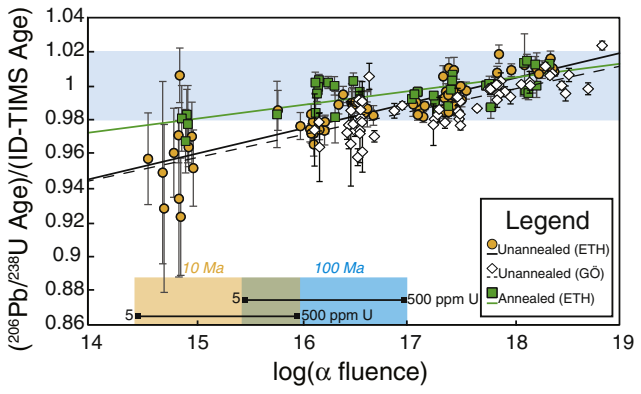

Fig. 3. Average $^{206}Pb/^{238}U$ LA-ICP-MS age offset vs log(dose) for all reference materials. Circles represent non-chemically abraded reference materials, while squares represent those that are chemically abraded. LA-ICP-MS data from Göttingen (GÖ) are plotted in diamonds for comparison. Each point represents the average (± 2 S.E.) of each reference material on each day. Below: Schematic representation of log(α dose) for samples aged 10 and 100 Ma from 5 to 500 μg g^{-1} U, demonstrating the range of zircons most affected by radiation damage-induced age offset.

the laser-generated aerosol, creating heterogeneous particle size distributions at the laser ablation site. While normalization to a primary reference material similar in matrix may correct for some of these effects, increased analytical precision has made it possible to observe that even very small differences in matrix properties between reference materials and samples impart significant analytical bias (Allen and Campbell, 2012; Marillo-Sialer et al., 2014).

The particle size distribution (PSD) of the ablated material differs between samples and matrices, leading to LIEF. The elemental and isotopic composition of different particle size fractions varies (Kuhn and Gunther, 2003), as does the PSD with time of a single hole ablation (Kozlov et al., 2003) and the PSD between different samples (Guillong and Gunther, 2002). For U-Pb dating, this is manifested as anomalously high Pb/U ratios in the smallest size fraction (Košler et al., 2005), which leads to older apparent ages (and conversely, younger ages for the larger size fractions). The PSD is created at the laser ablation site upon condensation from the laser plume, and because different size fractions have different vaporization, atomization and ionization efficiencies in the ICP, this ultimately determines the measured elemental and isotopic ratios.

Many approaches were investigated in the past to make LA-ICP-MS completely matrix-independent. The use of shorter wavelengths, particularly 193 nm (Günther and Heinrich, 1999a; Guillong et al., 2003a), as well as the use of He as an ablation gas (Eggins et al., 1998; Günther and Heinrich, 1999b) are well established methods to decrease the particle size and minimize LIEF. Unfortunately, zircon U-Pb ratios might be one of the most extreme and difficult examples of LIEF due to the large chemical and physical differences of the two elements and the fact that zircon partly separates into baddeleyite and quartz during laser ablation (Košler et al., 2005). Particles with different sizes also have different ionization efficiencies, leading to LIEF in the LA-ICP-MS process (Kroslakova and Günther, 2007). Aeschliman et al. (2003) were

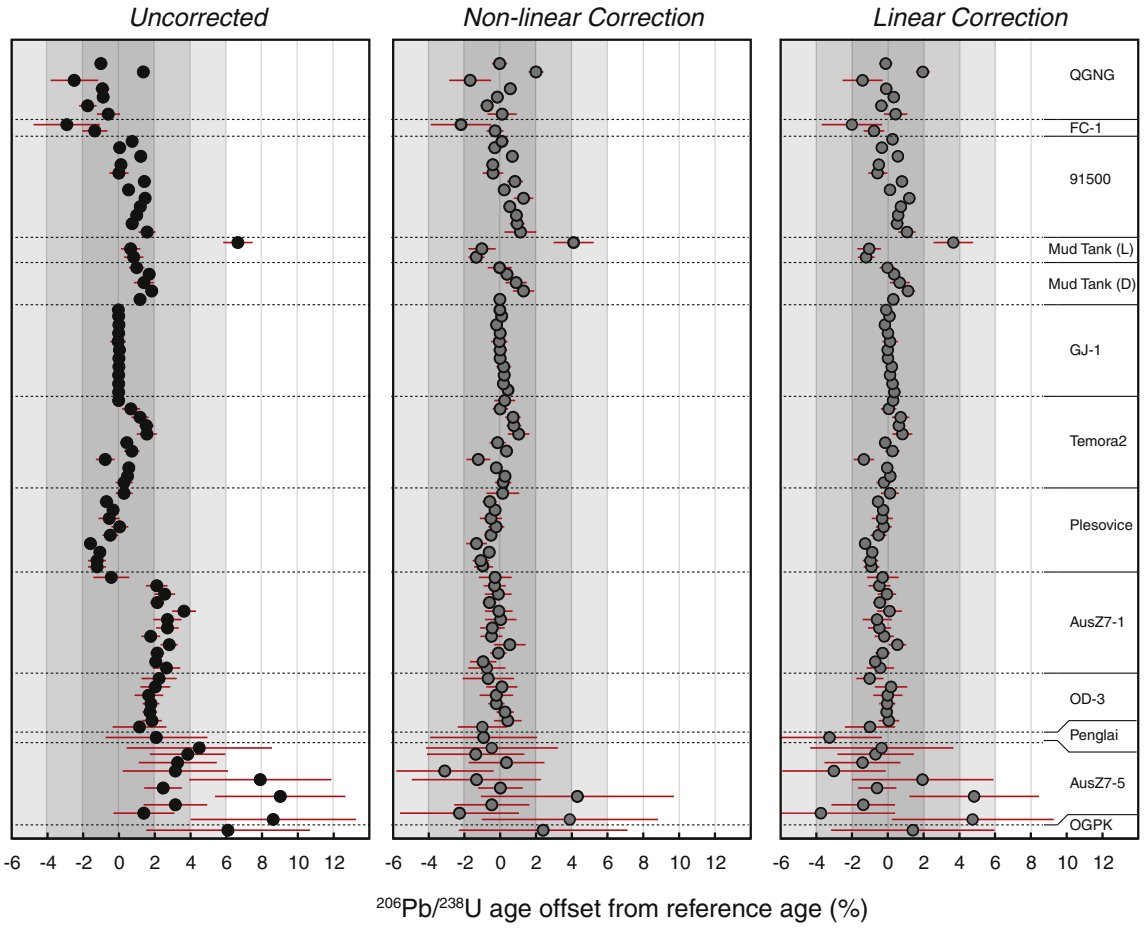

Fig. 4. Comparison of $^{206}Pb/^{238}U$ LA-ICP-MS ages with reference ages for zircon reference materials in the present study. Each data point represents pooled data (n = 8–25) from one session. Positive offset indicates younging, and data represent weighted mean ages of uncorrected, linearly-corrected and non-linearly-corrected data found in Table 4. Error bars represent 2 SE.

able to demonstrate that larger particles are incompletely ionized at the plasma source (potentially leading to LIEF), while Kuhn et al. (2004) were able to determine an optimal size fraction (90–150 nm) for complete ionization at a particular set of analytical parameters. Kuhn and Günther (2004) postulated that the source of LIEF lies predominantly at the plasma source and the incomplete ionization of larger particles, validating previous attempts to control the PSD by means of particle filters and other separation devices (Guillong and Gunther, 2002; Guillong et al., 2003b). However, because many of these studies are based on the ablation of glasses, some effects of post-ablation condensation were not considered. Namely, the condensation of baddeleyite from ablated zircon observed by Košler et al. (2005) fractionates U from Pb in a way that ablated glass does not. The efficiency of baddeleyite condensation may depend on the matrix properties of a given zircon, and can be different compared to the calibration reference material. Therefore, any efforts to homogenize PSD's would not eliminate this generally observed bias.

Analytical bias due to differences in matrix properties between reference materials and samples has been primarily attributed to small changes in “downhole fractionation.” This time- or crater depth-dependent U-Pb fractionation during laser drilling is proportional to the unique ablation rate of a given sample. This has in turn been attributed to differences in crystal lattice strengths (Allen and Campbell, 2012; Marillo-Sialer et al., 2014; Marillo-Sialer et al., 2016). Correction of resultant analytical biases is highly sought-after in the community, and has led to two general approaches:

The first approach is in fact a by-product of Pb-loss correction. Namely, matrix properties of zircon reference materials and the samples can be normalized by either thermal annealing (Nasdala et al., 2001; Allen and Campbell, 2012; Marillo-Sialer et al., 2014; Solari et al., 2015) or the entire chemical abrasion procedure (Crowley et al., 2014; von Quadt et al., 2014; Watts et al., 2016). Most notably, Allen and Campbell (2012) demonstrated that thermal annealing (850 °C for 48 h) was enough to reduce systematic bias among a variety of secondary standards (all > 400 Ma) to below 1%. Marillo-Sialer et al. (2016) noted that partial crystal lattice recovery was observed in Raman data following thermal annealing steps at 850 °C, with improved homogenization of ablation rates observed when annealing at 1000 °C. Chemically-abraded zircon reference materials in the present study behave consistently with the results of these authors, although some analytical bias is still present at the young (< 100 Ma) end of the age spectrum (Figs. 2, 3). Importantly, given that the analytical bias in this study persists in *young* zircons even *after* chemical abrasion, the authors suggest that this bias is not exclusively due to Pb loss as suggested by von Quadt et al. (2014), but mainly by greater lattice strength and slower ablation rates. This means that the lengthy process of chemical abrasion may effectively be replaced by thermal annealing alone. However, given that analytical biases in age *persist even after annealing*, the process may be avoided altogether in favor of a regression-based correction, thereby saving time and achieving a similar result.

Alternately, one may also try to identify and correct for the causes behind the remaining analytical bias. While such studies have been conducted (Marillo-Sialer et al., 2014; Marillo-Sialer et al., 2016), it should be noted that (1) the relationships between analytical bias and

Table 4
Comparison of correction techniques on reference materials.

		Measured				Corrected (non-linear)[a]				Corrected (linear)[a]			
Date	Reference material (n)	$^{206}Pb/^{238}U$ Age (Ma)	2 s (%)[c]	Age/std.[b]	MSWD	$^{206}Pb/^{238}U$ Age (Ma)	2 s (%)[c]	Age/std.[b]	MSWD	$^{206}Pb/^{238}U$ Age (Ma)	2 s (%)[a]	Age/std.[b]	MSWD
160527	91500 (8)	1047	1.4	0.984	1.2	1052	2.6	0.989	0.3	1052	1.4	0.989	1.2
160527	AusZ7-1 (8)	37.93	2.2	0.978	1.2	39.06	4.2	1.007	0.3	39.19	2.2	1.010	1.1
160527	GJ-1 (18)	602.0	1.4	1.000	0.6	600.4	2.5	0.998	0.2	600.1	1.4	0.997	0.6
160527	OD-3 (6)	32.62	1.8	0.988	2.6	33.33	3.5	1.010	0.6	33.33	1.9	1.010	2.2
160527	Plešovice (8)	338.6	1.4	1.004	2.8	338.1	2.7	1.003	0.6	338.1	1.5	1.003	2.1
160527	QGNG (8)	1853	1.2	1.006	1.6	1840	2.3	0.999	0.5	1834	0.7	0.996	1.6
160527	Temora2 (9)	415.6	1.4	0.997	1.0	416.2	2.7	0.999	0.2	416.3	1.4	0.999	0.8
160529	91500 (20)	1056	1.4	0.993	1.2	1053	1.9	0.991	1.0	1058	1.4	0.995	1.2
160529	AusZ7-1 (20)	37.77	3.6	0.973	0.9	39.09	4.9	1.007	0.6	38.98	3.6	1.005	0.9
160529	AusZ7-5 (20)	2.120	16	0.914	1.4	2.230	22	0.961	1.1	2.210	16	0.953	1.4
160529	GJ-1 (30)	602.0	1.4	1.000	0.3	599.3	1.8	0.996	0.2	599.7	1.4	0.996	0.3
160529	OD-3 (18)	32.39	2.5	0.982	1.1	32.86	3.4	0.996	0.5	32.98	2.5	0.999	0.9
160529	Plešovice (20)	341.3	1.4	1.012	2.2	340.3	1.9	1.009	1.4	340.2	1.4	1.009	1.7
160529	QGNG (17)	1874	1.2	1.017	2.7	1855	1.6	1.007	1.1	1849	1.2	1.004	1.2
160529	Temora2 (20)	415.6	1.6	0.997	1.7	416.1	2.1	0.998	0.8	417.7	1.6	1.002	1.3
160530	91500 (27)	1053	0.8	0.990	2.0	1054	1.6	0.991	0.7	1057	0.8	0.994	1.9
160530	AusZ7-1 (27)	38.00	1.8	0.977	0.9	38.25	4.1	0.984	0.2	39.14	1.8	1.006	1.0
160530	AusZ7-5 (27)	2.288	8.0	0.986	1.2	2.373	17	1.023	0.2	2.407	7.9	1.037	1.1
160530	GJ-1 (29)	602.0	0.7	1.000	0.5	600.8	1.5	0.998	0.1	600.3	0.7	0.997	0.5
160530	OD-3 (26)	32.43	1.3	0.983	2.7	32.97	2.8	0.999	0.8	33.09	1.3	1.003	1.2
160530	Plešovice (24)	341.3	0.8	1.012	9.3	340.8	1.6	1.011	2.0	340.4	0.8	1.010	7.7
160530	QGNG (26)	1858	0.7	1.009	3.4	1845	1.4	1.002	0.7	1836	0.7	0.997	2.8
160530	Temora2 (22)	414.8	0.8	0.995	3.3	415.7	1.6	0.997	0.9	416.2	0.8	0.999	2.7
160604	91500 (23)	1051	1.0	0.988	0.5	1058	1.3	0.995	0.3	1056	1.0	0.993	0.4
160604	AusZ7-1 (25)	37.97	1.8	0.976	1.2	38.91	2.4	1.001	0.8	38.99	1.8	1.003	1.2
160604	AusZ7-5 (25)	2.247	6.9	0.968	1.6	2.331	9.0	1.005	1.2	2.352	6.7	1.014	1.5
160604	FC-1 (25)	1115	1.0	1.014	13.0	1103	1.3	1.003	3.3	1108	1.0	1.008	8.3
160604	GJ-1 (46)	602.0	1.0	1.000	0.6	600.5	1.3	0.998	0.3	601.17	1.0	0.999	0.6
160604	MT dark (25)	723.0	1.1	0.988	1.0	731.8	1.5	1.000	0.6	729.4	1.1	0.997	1.0
160604	MT light (25)	725.6	1.8	0.992	2.2	741.4	2.4	1.013	1.1	740.5	1.8	1.012	1.7
160604	OD-3 (23)	32.41	1.5	0.982	2.2	33.14	2.0	1.004	1.2	33.09	1.5	1.003	2.2
160604	OGPK (21)	0.939	14	0.939	2.7	0.976	19	0.976	1.5	0.986	14	0.986	2.6
160604	Penglai (25)	4.21	11	0.979	1.6	4.340	15	1.009	0.9	4.440	11	1.033	1.5
160604	Plešovice (24)	340.8	1.0	1.011	1.5	339.2	1.3	1.006	0.8	340.1	1.0	1.009	1.2
160604	QGNG (24)	1859	0.9	1.009	4.1	1832	1.2	0.994	1.9	1844	0.9	1.001	3.0
160604	Temora2 (24)	414.5	1.1	0.994	1.6	417.7	1.4	1.002	0.8	416.9	1.1	1.000	1.4
160608	91500 (15)	1048	1.2	0.985	1.0	1050	2.2	0.987	0.3	1051	1.2	0.988	1.1
160608	AusZ7-1 (15)	37.71	1.9	0.970	0.6	38.66	3.6	0.994	0.2	38.66	1.9	0.994	0.6
160608	AusZ7-5 (15)	2.111	13	0.910	1.4	2.220	23	0.957	0.5	2.208	12	0.952	1.3
160608	FC-1 (14)	1132	1.1	1.029	30.0	1124	2.1	1.022	8.0	1122	1.2	1.020	25.0
160608	GJ-1 (26)	601.9	1.2	1.000	0.8	600.7	2.2	0.998	0.2	600.5	1.2	0.998	0.7
160608	MT dark (17)	718.2	1.3	0.982	1.0	722.1	2.4	0.987	0.4	723.3	2.2	0.989	1.2
160608	MT light (15)	726.9	1.7	0.994	1.5	739.1	3.3	1.010	0.8	739.3	1.8	1.010	2.3
160608	OD-3 (10)	32.45	1.7	0.983	1.6	33.15	3.1	1.005	1.1	33.08	1.7	1.002	1.6
160608	Plešovice (15)	342.5	1.2	1.016	1.1	341.6	2.3	1.013	0.4	341.4	1.3	1.013	1.1
160608	QGNG (14)	1888	1.1	1.025	18.0	1873	2.0	1.017	4.3	1868	1.1	1.014	13.0
160608	Temora2 (12)	420	1.3	1.008	1.5	421.9	2.4	1.012	0.6	422.4	1.3	1.013	1.9
160711	91500 (10)	1058	0.9	0.995	0.7	1061	1.1	0.998	0.6	1062	0.9	0.999	0.8
160711	AusZ7-1 (14)	38.11	1.4	0.980	1.6	38.99	1.7	1.003	1.6	38.88	1.4	1.000	1.6
160711	AusZ7-5 (15)	2.263	4.2	0.975	1.1	2.320	4.9	1.000	0.8	2.334	4.2	1.006	1.1
160711	GJ-1 (32)	601.9	0.9	1.000	0.8	601.9	1.0	1.000	0.6	601.8	0.9	1.000	0.8
160711	Plešovice (11)	338.8	1.1	1.005	1.6	338.9	1.3	1.005	1.2	338.9	1.1	1.005	1.6
160711	Temora2 (9)	413.8	0.9	0.993	1.5	415.3	1.1	0.996	1.0	415.7	0.9	0.997	1.4
160731	91500 (18)	1048	1.5	0.986	0.8	1055	1.9	0.992	0.4	1055	1.5	0.992	0.6
160731	AusZ7-1 (20)	37.75	2.4	0.971	1.2	38.97	3.2	1.002	0.7	38.98	2.5	1.002	1.2
160731	GJ-1 (22)	601.7	1.4	1.000	0.8	601.9	1.8	1.000	0.5	601.9	1.4	1.000	0.8
160731	Plešovice (19)	337	1.5	1.000	1.6	337.9	1.9	1.002	1.0	337.9	1.5	1.002	1.5
160731	Temora2 (20)	415	1.6	0.996	1.0	417.4	2.1	1.001	0.5	417.4	1.6	1.001	0.8
161010	91500 (15)	1064	2.1	1.000	0.7	1068	2.2	1.004	0.7	1070	2.1	1.006	0.8
161010	AusZ7-1 (15)	37.75	3.2	0.971	1.2	38.79	3.5	0.997	1.1	39.03	3.3	1.004	1.1
161010	AusZ7-5 (15)	2.137	12	0.921	1.4	2.351	14	1.013	1.1	2.275	12	0.981	1.4
161010	GJ-1 (23)	602.2	2.1	1.000	0.9	602.2	2.3	1.000	0.7	601.1	2.1	0.999	0.8
161010	MT dark (15)	721.5	2.2	0.986	0.9	725.1	2.3	0.991	0.8	726.8	2.2	0.993	1.0
161010	MT light (15)	683	3.2	0.934	1.1	701.6	3.5	0.959	1.4	704.8	3.2	0.963	1.6
161010	Plešovice (13)	339	2.1	1.005	0.9	338.9	2.3	1.005	0.8	338.2	2.1	1.003	0.9
161010	Temora2 (15)	410.3	2.2	0.984	1.2	412.5	2.4	0.990	1.0	413.4	2.2	0.992	1.1
161016	91500 (20)	1062	1.1	0.999	1.4	1068	1.4	1.004	0.9	1069	1.1	1.005	1.3
161016	AusZ7-1 (19)	37.39	2.0	0.961	1.8	38.83	2.9	0.998	1.3	38.76	2.1	0.997	1.9
161016	AusZ7-5 (19)	2.247	8.5	0.968	2.1	2.392	12	1.031	1.1	2.390	8.1	1.030	2.0
161016	GJ-1 (56)	602.0	1.1	1.000	0.9	601.9	1.4	1.000	0.5	601.8	1.1	1.000	0.9
161016	MT dark (20)	719.3	1.2	0.983	1.6	728.9	1.6	0.996	0.9	729.1	1.2	0.997	1.6
161016	Plešovice (18)	338.2	1.1	1.003	0.8	338.1	1.4	1.003	0.4	338	1.1	1.003	0.8

(*continued on next page*)

Table 4 (*continued*)

Date	Reference material (n)	Measured				Corrected (non-linear)[a]				Corrected (linear)[a]			
		$^{206}Pb/^{238}U$ Age (Ma)	2 s (%)[c]	Age/std.[b]	MSWD	$^{206}Pb/^{238}U$ Age (Ma)	2 s (%)[c]	Age/std.[b]	MSWD	$^{206}Pb/^{238}U$ Age (Ma)	2 s (%)[a]	Age/std.[b]	MSWD
161016	QGNG (19)	1817	1.0	0.986	1.6	1805	1.4	0.980	1.5	1806	1.0	0.980	2.5
161016	Temora2 (19)	410.4	1.1	0.985	2.4	413.6	1.5	0.992	1.3	414.2	1.1	0.994	1.7
161204	91500 (22)	1051	1.0	0.988	1.0	1056	1.2	0.993	0.7	1058	1.0	0.994	1.0
161204	AusZ7-1 (23)	37.97	1.5	0.976	1.3	39.03	1.9	1.004	1.1	38.97	1.6	1.002	1.3
161204	AusZ7-5 (23)	2.244	8.6	0.967	1.4	2.312	10	0.996	1.0	2.353	8.4	1.014	1.3
161204	GJ-1 (48)	601.9	0.9	1.000	0.8	603.1	1.1	1.002	0.5	602.8	0.9	1.002	0.8
161211	91500 (19)	1063	1.5	1.000	0.5	1067	1.8	1.003	0.5	1067	1.4	1.003	0.7
161211	AusZ7-1 (19)	37.81	2.7	0.972	0.9	38.84	3.4	0.999	0.6	38.82	2.8	0.998	0.9
161211	AusZ7-5 (19)	2.231	9.6	0.962	1.0	2.352	12	1.014	0.6	2.336	9.6	1.007	1.0
161211	GJ-1 (53)	602.0	1.4	1.000	0.9	601.4	1.7	0.999	0.6	601.3	1.4	0.999	0.9
161211	MT dark (18)	724.4	1.8	0.990	1.0	731.9	2.3	1.000	1.5	731.8	1.9	1.000	2.2
161211	OD-3 (20)	32.33	2.1	0.980	3.0	32.97	2.6	0.999	2.0	32.94	2.1	0.998	2.8
161211	Plešovice (17)	339.5	1.4	1.007	1.2	339.1	1.7	1.006	0.8	339	1.4	1.005	1.1
161211	QGNG (14)	1861	1.4	1.010	0.2	1843	1.7	1.000	0.2	1844	1.4	1.001	0.3
161211	Temora2 (18)	411.9	1.5	0.988	1.7	413.8	1.9	0.993	1.1	413.8	1.5	0.993	1.7
170713	91500 (15)	1056	1.0	0.993	1.4	1063	1.2	0.999	1.2	1061	1.0	0.997	1.1
170713	AusZ7-1 (15)	37.98	1.9	0.977	1.3	38.92	2.4	1.001	0.9	38.98	2.0	1.002	1.3
170713	AusZ7-5 (15)	2.216	12	0.955	1.6	2.331	14	1.005	1.0	2.328	11	1.003	1.5
170713	GJ-1 (20)	602.1	0.9	1.000	0.8	602	1.1	1.000	0.5	602.4	0.9	1.001	0.8
170713	Temora2 (15)	414.0	1.0	0.993	3.1	416.8	1.2	1.000	1.7	416.6	1.0	1.000	2.3

[a] Corrected for alpha dose.
[b] LA-ICP-MS U-Pb age divided by standard reference age (uncorrected for Th disequilibrium).
[c] Average relative uncertainty on spot analysis.

Table 5
Comparison of age correction techniques on young igneous units.

Date	Sample	Measured				Corrected (non-linear)[a]				Corrected (linear)[a]			
		$^{206}Pb/^{238}U$ Age (Ma)	2 s (%)[c]	Age/std.[b]	MSWD	$^{206}Pb/^{238}U$ Age (Ma)	2 s (%)[c]	Age/std.[b]	MSWD	$^{206}Pb/^{238}U$ Age (Ma)	2 s (%)[c]	Age/std.[b]	MSWD
161204	Rat Creek $n = 61$	26.56	1.7	0.987	3.8	27.39	2.2	1.018	2.4	27.28	1.7	1.014	3.8
161211	Fish Canyon $n = 50$	27.84	2.3	0.987	4.5	28.38	2.8	1.006	3.4	28.33	2.6	1.005	4.6
170713	La Gloria (LG0103) $n = 22$	11.04	2.4	0.982	2.3	11.38	3.0	1.013	1.8	11.37	2.4	1.011	2.4

[a] Corrected for alpha dose.
[b] LA-ICP-MS U-Pb age divided by standard reference age (uncorrected for Th disequilibrium).
[c] Average relative uncertainty on spot analysis.

factors such as color, orientation and chemical composition remain complex and difficult to predict; and (2) any efforts to determine these factors either adds significantly more work (e.g. by grain orientation or EBSD measurements) or decreases analytical precision (e.g. simultaneous U-Pb analysis with trace elements). A simpler correction scheme based purely on U and Th concentrations (i.e. Dose_Corrector) is therefore warranted.

In light of recent community-based recommendations for LA-ICP-MS U-Pb dating (Horstwood et al., 2016), it is necessary to address how Dose_Corrector would change the typical workflow, and how systematic uncertainties from alpha dose regressions are propagated. Given that the DRS takes effect after downhole fractionation and drift correction (and after common Pb correction, if implemented), it should take place after step 7 (i.e., after individual age calculation; see Fig. 1 of Horstwood et al., 2016). The uncertainties derived from confidence bands of the regression line (this study) and from the Th disequilibrium correction can be treated as random uncertainties and can therefore be propagated into the data point uncertainty (i.e., the $^{206}Pb/^{238}U$ age uncertainty). However, because the DRS aims to correct for analytical bias, the remainder of the workflow regarding systematic uncertainties requires a different approach. Long-term excess variance of validation materials (ε') can be calculated following the examples of Horstwood et al. (2016) and Matthews and Guest (2017), wherein uncertainty is added to each data point until the MSWD of the population of a homogeneous reference material is ~1. Application of this approach over 12 sessions yielded 0.2% and 0.6% excess uncertainty on the $^{206}Pb/^{238}U$ ratio for AusZ7–1 and 91500, respectively (Fig. 6). However, propagating this uncertainty does not improve the accuracy of the age determinations. An alternative approach to quantifying uncertainty while improving accuracy is also shown here, taking advantage of the multiple reference materials analyzed.

4.1. Propagation of uncertainty from alpha dose correction

Traditionally, uncertainty calculations start with the variability in the ratio of the calibration reference material, and proceed to quadratically propagate additional sources of uncertainty due to downhole fractionation correction, reference material normalization, common Pb correction, etc. Using this approach, one can propagate the uncertainty of the dose correction using the 95% confidence bands of the regression line as a proxy for 2s error. Because of the relatively high precision on the regression, however, the change in uncertainty due to the dose

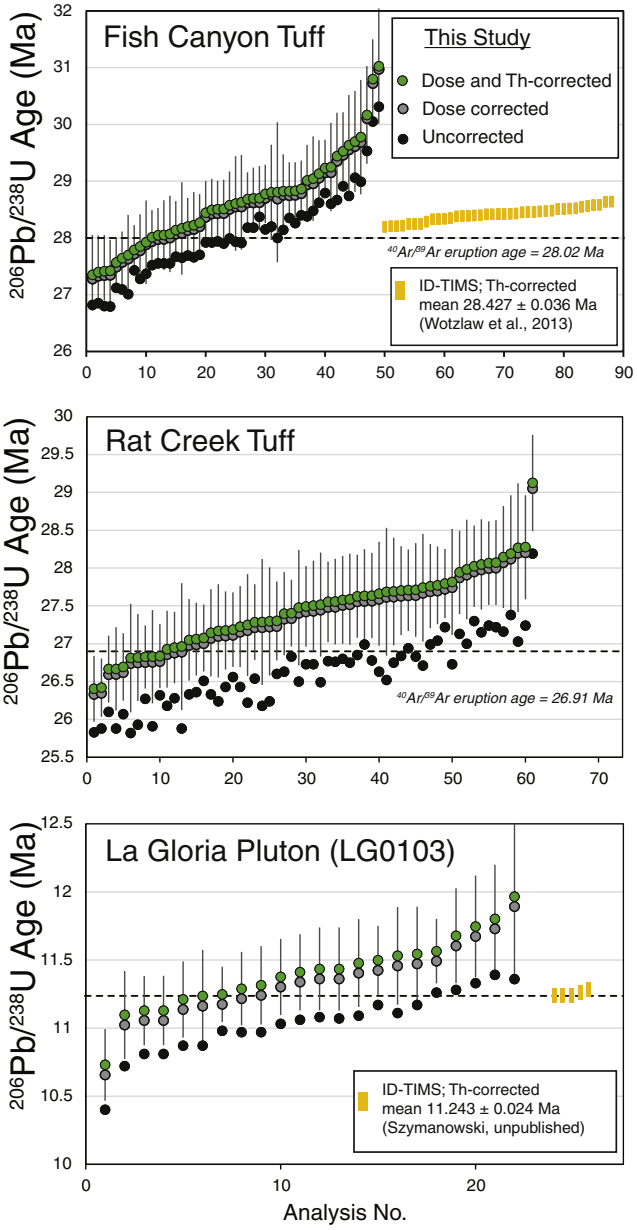

Fig. 5. Zircon U-Pb data from the Fish Canyon Tuff, Rat Creek Tuff and La Gloria Pluton, rank ordered. Left: uncorrected data (primary iolite output), dose-corrected (non-linear model) data and data corrected for both alpha radiation dose and Th disequilibrium. Right: Literature CA-ID-TIMS analyses. $^{40}Ar/^{39}Ar$ eruption ages are from Phillips and Matchan (2013) and Lipman and McIntosh (2008) for Fish Canyon and Rat Creek Tuffs, respectively. Error bars on ID-TIMS ages are smaller than the symbol.

correction is negligible (Fig. 7a), which raises a problematic issue: it has been demonstrated that variations in matrix properties are responsible for analytical biases in age determinations, so why not assume that differing matrix properties *within* a standard reference material can also impart systematic bias? Reference materials are often large, homogeneous grains (e.g. GJ-1, 91500, Mud Tank), and the excess scatter that is propagated from these grains may not reflect the amount of excess scatter in more heterogeneous reference materials (e.g. Temora, Plešovice). In other words, while data reduction may lead to a mean square weighted deviates (MSWD) close to 1 for calibration reference materials (indicating a homogeneous age population with an accurately calculated uncertainty), it may be in excess of 1 in validation reference materials (indicating underestimation of uncertainty).

In a single analytical session, the age of each reference material analysis is a function of (1) the $^{206}Pb/^{238}U$ therein (corrected for mass bias and elemental fractionation); (2) the internal uncertainty of the signal, which contributes to the random scatter around the mean and (3) excess scatter, which may be due to matrix effects, variations in plasma conditions, etc. As an example, if a number of points are measured from a reference material with a homogeneous age, one can expect to see a normally-distributed sample of ages, where 95% of the analyses are within 2s of the mean. By necessity, the standard deviation of the sample population is equal to the standard deviation of each individual analysis. However, if *multiple* standard reference materials are analyzed, then the same may not be true due to variability in the amounts of excess scatter between calibration and validation reference materials (as explained above). Fortunately, because there are multiple standards, there are also multiple points of reference where data can be validated.

If it is true that a linear regression through multiple standard reference materials adequately corrects for systematic age bias, then a set of 95% prediction bands around the regression should capture 95% of all data points and therefore represent 2s uncertainty. This approach would differ drastically from the traditional method, as it involves no propagation of uncertainty, and is instead empirically determined on a suite of reference materials which are known to have homogeneous ages. A quick examination of the prediction bands on a linear regression model, however, reveal that this approach is inadequate in the case of a linear regression (Fig. 7a). While the prediction bands *do* encompass 95% of the data, it is clear that the error on high-dose samples is overestimated, while the error on low-dose samples is overestimated. If the prediction bands are to represent 2s uncertainty, then one must also consider that uncertainty is a function of log(α dose). In other words, with low dose, the relative uncertainty on measurements becomes exponentially greater, and can be modelled as such (Fig. 8).

It has already been established that the analytical bias in $^{206}Pb/^{238}U$ can be modeled by a linear equation (Allen and Campbell, 2012):

$$f(x) = ax + b \tag{2}$$

where x denotes the log(α dose). The relative uncertainty, meanwhile, follows an exponential curve which increases at low log(α dose) (Fig. 8):

$$f(x) = c + de^{fx} \tag{3}$$

The two equations can be combined:

$$f(x) = \frac{ax + b}{c + de^{fx}} \tag{4}$$

where f(x) represents the % deviation from true age, x represents the log(α dose) and a, b, c, d and f represent constants. If one takes the age offset of an analysis and divides by the relative uncertainty on that analysis, one can theoretically generate an array of data that can be fit by Eq. (4). That is:

$$\frac{1 - \frac{age_{meas}}{age_{corr}}}{\sigma} = f(x) = \frac{ax + b}{c + de^{fx}}$$

where age_{meas} is the measured age, age_{corr} is the reference age, and σ is the relative uncertainty provided by primary data reduction. Here one can solve for age_{corr}:

$$age_{corr} = \frac{age_{meas}}{(1 - f(x)^{*}\sigma)} \tag{5}$$

By normalizing the age offset with the relative uncertainty, the data scatter becomes independent of log(α dose). Importantly, one can now generate prediction bands around the regression curve in Eq. (4), which encompass 95% of all data points, and therefore represent 2s uncertainty which is determined on *multiple reference materials* (Fig. 7b). This uncertainty is greater than the propagated uncertainty of a homogeneous standard reference material, as it captures the excess

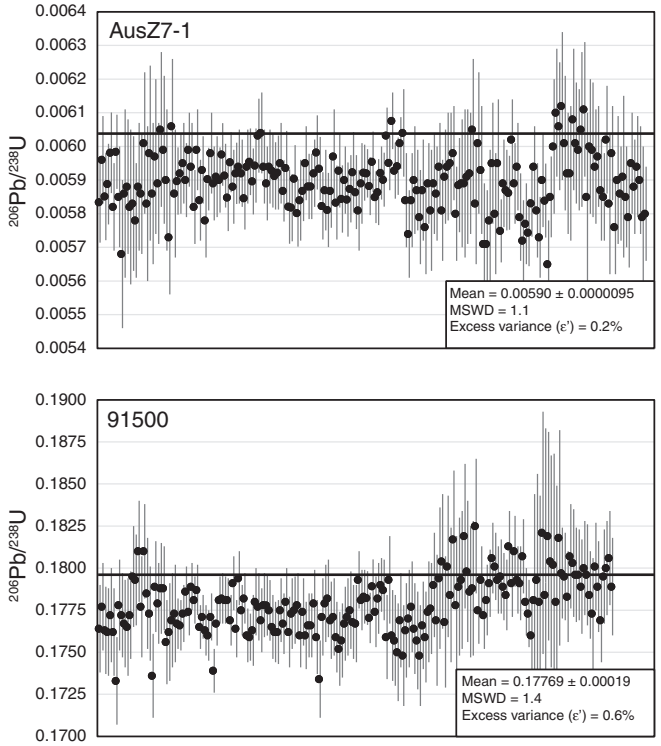

Fig. 6. Estimation of long-term excess variance of validation reference materials using two homogeneous zircons: AusZ7-1 and 91500. Horizontal black bars represent reference $^{206}Pb/^{238}U$ from ID-TIMS, while error bars denote 2 s on LA-ICP-MS measurements (uncorrected for radiation dose). The weighted mean and 2 s uncertainty are provided in the lower right along with an MSWD for each population, having rejected 8/197 (4.1%) of data from AusZ7-1 and 9/189 (4.8%) of data from 91500.

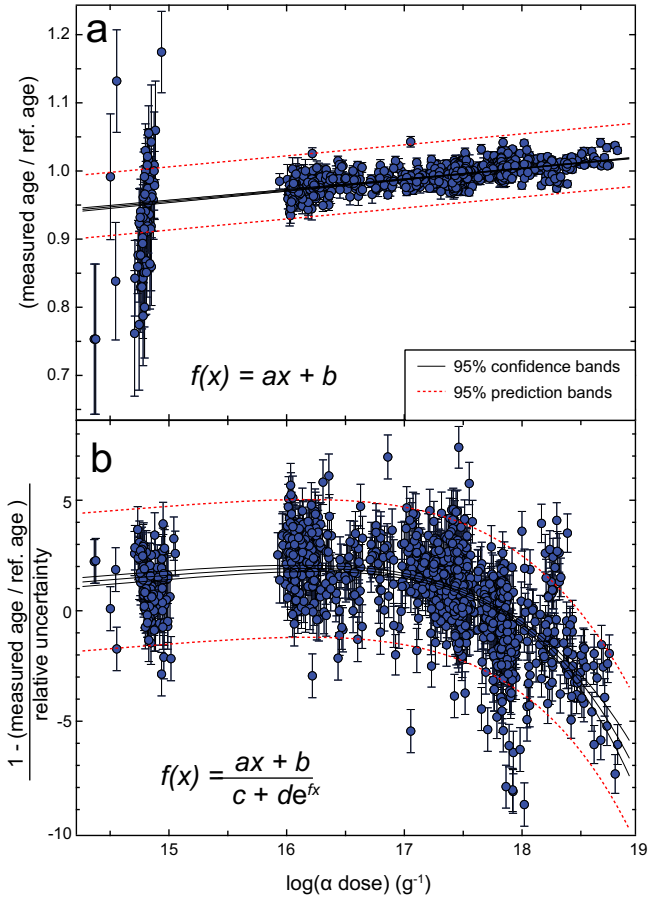

Fig. 7. Comparison of regression models on all data from this study: (a) linear model with 95% confidence and prediction bands for all data in the present study. Note the overestimation of uncertainty at the right side of the graph. (b) combined linear/exponential model, with prediction bands reliably encompassing 95% of all data without appreciable over- or underestimation at either end. Equations denote the regression formulas used in each model, where a, b, c, d and f denote constants.

uncertainty of multiple heterogeneous reference materials.

The utility of this method becomes clear when addressing questions about timescales of geological processes. For example, magmatic differentiation times are frequently assessed using U-(Th)-Pb geochronology in zircons (Schoene et al., 2012; Wotzlaw et al., 2013). While ID-TIMS is the method of choice and provides the greatest precision, it may also be possible to utilize the high sample throughput of LA-ICP-MS to obtain useful information about residence times as well—provided that analytical biases have been eliminated. Many labs are able to produce data with an uncertainty of ~1% 2s, but if matrix effects contribute additional uncertainty to the scatter of a data population, then the MSWD of such a population will be erroneously high and may suggest extremely protracted residence times. Modifying the uncertainty of these populations to remain consistent with multiple standard reference materials may be a viable way to generate a more realistic MSWD and to extract more meaningful information out of age spectra.

4.2. Application

The correction scheme in the present study is designed for Cenozoic zircons, with the term "Cenozoic" used semi-arbitrarily to denote young zircons that contain less than $\sim 10^{16}$ decays per gram. Here, the analytical biases associated with using old reference materials (e.g. 91500, GJ-1) become increasingly pronounced and consistent between analytical sessions. Unfortunately, it is precisely the young zircons which are often at the focus of volcanological research, as researchers tend to work on well-exposed, unweathered units, and additionally take interest in magmatic residence times that are only resolvable at young ages. Therefore, a correction scheme is necessary to reconcile U-Pb LA-ICP-MS zircon data with independent measures of age such as $^{40}Ar/^{39}Ar$ ages. However, there is a benefit to studying young zircons in that one is more confident about the thermal history of the units under study. It has been demonstrated that thermal annealing reduces analytical bias in a laboratory setting, but it equally true that thermal events (i.e. metamorphism) in the history of a zircon may impart similar annealing effects, which would make that zircon appear systematically younger than its true age if compared to an unannealed reference material. Young zircons are less likely to have undergone a protracted history of burial, metamorphism and exhumation, and one can usually assume that they plot accurately on the age offset vs log(α dose) graph.

The dose correction scheme in this study is validated on several Cenozoic zircon suites: the La Gloria Pluton (11 Ma), the Rat Creek Tuff

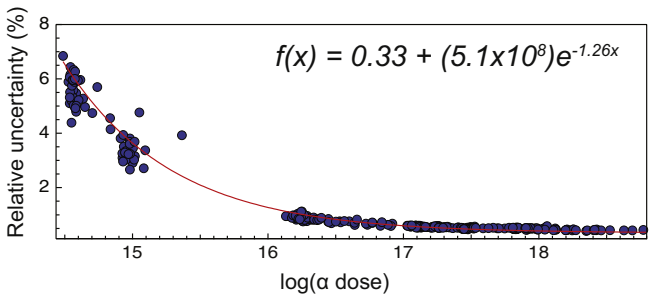

Fig. 8. Exponential regression line modeling the relationship between log(Dose) and relative uncertainty. Data are from 4 Jun 2016.

Dacite (26.9 Ma) and the 28 Ma Fish Canyon Tuff (Fig. 5). $^{40}Ar/^{39}Ar$ eruption ages in the latter two units provide strict lower limits to zircon ages, which are consistent with the youngest subpopulations of dose-corrected zircons. In the former case, slower cooling of the pluton inhibits the application of $^{40}Ar/^{39}Ar$ dating, but the ID-TIMS ages from zircons provide a reference point for LA analysis. Indeed, dose-corrected ages are more consistent with the ID-TIMS ages, further validating the method.

5. Conclusions

This study examines the effects of total alpha dose in zircon on systematic biases in U-Pb age determination by LA-ICP-MS. In particular:

1. We demonstrate the dependence of age offsets on the total alpha dose experienced by reference zircons (calculated using the U and Th concentrations and the reference age).
2. We propose that such systematic biases can be corrected using a linear regression model, but the analysis of several secondary standards (ideally, 10–20 analysis of > 5 secondary reference materials) throughout the day is essential in defining such a regression.
3. Systematic bias toward younger LA-ICP-MS dates in low alpha damage density zircons is likely not due to Pb-loss alone, but is rather caused by matrix effects. For this reason, chemical abrasion can be foregone in favor of thermal annealing in order to improve data accuracy and scatter.
4. Because systematic younging cannot be completely eliminated by chemical abrasion or thermal annealing, one may instead choose to correct age data by regression alone. An iolite add-on (Dose_corrector.ipf) is presented, which facilitates data reduction and application of two different regression models.
5. Analysis of non-chemically abraded Fish Canyon Tuff, Rat Creek Tuff and La Gloria pluton zircons and subsequent correction yielded age data consistent with ID-TIMS data and/or $^{40}Ar/^{39}Ar$ eruptions ages.
6. A new method of quantifying uncertainty is presented, which forgoes error propagation in favor of empirically-derived uncertainties validated on multiple (ideally, chemically heterogeneous) reference materials.

Supplementary data to this article can be found online at http://dx.doi.org/10.1016/j.chemgeo.2017.09.014.

Acknowledgments

This work was supported by ETH Research Grant ETH-34 15-2. We would like to thank Dawid Szymanowski for providing ID-TIMS data for sample LG0103 and Francisco Gutierrez for providing the sample. CL imaging was conducted at the Scientific Center for Optical and Electron Microscopy (ScopeM) at ETHZ. We thank William Matthews and an anonymous reviewer for constructive reviews.

References

Aeschliman, D.B., Bajic, S.J., Baldwin, D.P., Houk, R., 2003. High-speed digital photographic study of an inductively coupled plasma during laser ablation: comparison of dried solution aerosols from a microconcentric nebulizer and solid particles from laser ablation. J. Anal. At. Spectrom. 18 (9), 1008–1014.

Allen, C.M., Campbell, I.H., 2012. Identification and elimination of a matrix-induced systematic error in LA-ICP-MS Pb-206/U-238 dating of zircon. Chem. Geol. 332, 157–165. http://dx.doi.org/10.1016/j.chemgeo.2012.09.038.

Bachmann, O., Charlier, B.L.A., Lowenstern, J.B., 2007. Zircon crystallization and recycling in the magma chamber of the rhyolitic Kos Plateau Tuff (Aegean arc). Geology 35 (1), 73–76. http://dx.doi.org/10.1130/G23151a.1.

Barboni, M., Boehnke, P., Schmitt, A.K., Harrison, T.M., Shane, P., Bouvier, A.-S., Baumgartner, L., 2016. Warm storage for arc magmas. Proc. Natl. Acad. Sci. U. S. A. http://dx.doi.org/10.1073/pnas.1616129113.

Black, L., Gulson, B., 1978. The age of the mud tank carbonatite, strangways range, northern territory. BMR J. Aust. Geol. Geophys. 3 (3), 227–232. http://dx.doi.org/10.1007/BF00283322.

Black, L.P., Kamo, S.L., Williams, I.S., Mundil, R., Davis, D.W., Korsch, R.J., Foudoulis, C., 2003. The application of SHRIMP to Phanerozoic geochronology; a critical appraisal of four zircon standards. Chem. Geol. 200 (1–2), 171–188. http://dx.doi.org/10.1016/S0009-2541(03)00166-9.

Black, L.P., Kamo, S.L., Allen, C.M., Davis, D.W., Aleinikoff, J.N., Valley, J.W., Mundil, R., Campbell, I.H., Korsch, R.J., Williams, I.S., Foudoulis, C., 2004. Improved (206)Pb/(238)U microprobe geochronology by the monitoring of a trace-element-related matrix effect; SHRIMP, ID-TIMS, ELA-ICP-MS and oxygen isotope documentation for a series of zircon standards. Chem. Geol. 205 (1–2), 115–140. http://dx.doi.org/10.1016/j.chemgeo.2004.01.003.

Buret, Y., von Quadt, A., Heinrich, C., Selby, D., Walle, M., Peytcheva, I., 2016. From a long-lived upper-crustal magma chamber to rapid porphyry copper-emplacement: reading the_geochemistry of zircon crystals at Bajo de la Alumbrera (NW Argentina). Earth Planet. Sci. Lett. 450, 120–131. http://dx.doi.org/10.1016/j.epsl.2016.06.017.

Buret, Y., Wotzlaw, J.-F., Roozen, S., Guillong, M., von Quadt, A., Heinrich, C.A., 2017. Zircon petrochronological evidence for a plutonic-volcanic connection in porphyry copper deposits. Geology 45 (7), 623–626.

Chakoumakos, B.C., Murakami, T., Lumpkin, G.R., Ewing, R.C., 1987. Alpha-decay induced fracturing in zircon - the transition from the crystalline to the Metamict state. Science 236 (4808), 1556–1559. http://dx.doi.org/10.1126/science.236.4808.1556.

Channell, J.E.T., Hodell, D.A., Singer, B.S., Xuan, C., 2010. Reconciling astrochronological and Ar-40/Ar-39 ages for the Matuyama-Brunhes boundary and late Matuyama Chron. Geochem. Geophys. Geosyst. 11. http://dx.doi.org/10.1029/2010gc003203.

Chelle-Michou, C., Chiaradia, M., Ovtcharova, M., Ulianov, A., Wotzlaw, J.-F., 2014. Zircon petrochronology reveals the temporal link between porphyry systems and the magmatic evolution of their hidden plutonic roots (the Eocene Coroccohuayco deposit, Peru). Lithos 198, 129–140.

Claiborne, L.L., Miller, C.F., Flanagan, D.M., Clynne, M.A., Wooden, J.L., 2010. Zircon reveals protracted magma storage and recycling beneath Mount St. Helens. Geology 38 (11), 1011–1014. http://dx.doi.org/10.1130/G31285.1.

Cooper, K.M., Kent, A.J.R., 2014. Rapid remobilization of magmatic crystals kept in cold storage. Nature 506 (7489), 480–483. http://dx.doi.org/10.1038/nature12991.

Crowley, Q.G., Heron, K., Riggs, N., Kamber, B., Chew, D., McConnell, B., Benn, K., 2014. Chemical abrasion applied to LA-ICP-MS U-Pb zircon geochronology. Mineral-Basel 4 (2), 503–518. http://dx.doi.org/10.3390/min4020503.

Eggins, S.M., Kinsley, L.P.J., Shelley, J.M.G., 1998. Deposition and element fractionation processes during atmospheric pressure laser sampling for analysis by ICP-MS. Appl. Surf. Sci. 127, 278–286. http://dx.doi.org/10.1016/S0169-4332(97)00643-0.

Gehrels, G.E., Valencia, V.A., Ruiz, J., 2008. Enhanced precision, accuracy, efficiency, and spatial resolution of U-Pb ages by laser ablation-multicollector-inductively coupled plasma-mass spectrometry. Geochem. Geophys. Geosyst. 9. http://dx.doi.org/10.1029/2007gc001805.

Gerdes, A., Zeh, A., 2006. Combined U–Pb and Hf isotope LA-(MC-) ICP-MS analyses of detrital zircons: comparison with SHRIMP and new constraints for the provenance and age of an Armorican metasediment in Central Germany. Earth Planet. Sci. Lett. 249 (1), 47–61.

Guillong, M., Gunther, D., 2002. Effect of particle size distribution on ICP-induced elemental fractionation in laser ablation-inductively coupled plasma-mass spectrometry. J. Anal. At. Spectrom. 17 (8), 831–837. http://dx.doi.org/10.1039/b202988j.

Guillong, M., Horn, I., Günther, D., 2003a. A comparison of 266 nm, 213 nm and 193 nm produced from a single solid state Nd: YAG laser for laser ablation ICP-MS. J. Anal. At. Spectrom. 18 (10), 1224–1230.

Guillong, M., Kuhn, H.-R., Günther, D., 2003b. Application of a particle separation device to reduce inductively coupled plasma-enhanced elemental fractionation in laser ablation-inductively coupled plasma-mass spectrometry. Spectrochim. Acta B At. Spectrosc. 58 (2), 211–220.

Guillong, M., von Quadt, A., Sakata, S., Peytcheva, I., Bachmann, O., 2014. LA-ICP-MS Pb–U dating of young zircons from the Kos–Nisyros volcanic centre, SE Aegean arc. J. Anal. At. Spectrom. 29 (6), 963–970.

Guillong, M., Sliwinski, J.T., Schmitt, A., Forni, F., Bachmann, O., 2016. U-Th zircon dating by laser ablation single collector inductively coupled plasma-mass spectrometry (LA-ICP-MS). Geostand. Geoanal. Res. 40 (3), 377–387. http://dx.doi.org/10.1111/j.1751-908X.2016.00396.x.

Günther, D., Heinrich, C.A., 1999Fa. Comparison of the ablation behaviour of 266 nm Nd: YAG and 193 nm ArF excimer lasers for LA-ICP-MS analysis. J. Anal. At. Spectrom. 14 (9), 1369–1374.

Günther, D., Heinrich, C.A., 1999Fb. Enhanced sensitivity in laser ablation-ICP mass spectrometry using helium-argon mixtures as aerosol carrier. J. Anal. At. Spectrom. 14 (9), 1363–1368.

Gutierrez, F.J., Bachmann, O., Parada, M.A., Payacán, I., Gelman, S.E., 2013. Late-stage magma flow in a shallow felsic reservoir: merging the anisotropy of magnetic susceptibility record with numerical simulations in La Gloria Pluton, central Chile. J. Geophys. Res. 118, 1–15. http://dx.doi.org/10.1002/jgrb.50164.

Horn, I., von Blanckenburg, F., 2007. Investigation on elemental and isotopic fractionation during 196 nm femtosecond laser ablation multiple collector inductively coupled plasma mass spectrometry. Spectrochim. Acta B At. Spectrosc. 62 (4), 410–422.

Horstwood, M.S., Košler, J., Gehrels, G., Jackson, S.E., McLean, N.M., Paton, C., Pearson, N.J., Sircombe, K., Sylvester, P., Vermeesch, P., 2016. Community-derived standards for LA-ICP-MS U-(Th-) Pb geochronology–uncertainty propagation, age interpretation and data reporting. Geostand. Geoanal. Res. http://dx.doi.org/10.1111/j.1751-908X.2016.00379.x.

Iwano, H., Orihashi, Y., Hirata, T., Ogasawara, M., Danhara, T., Horie, K., Hasebe, N., Sueoka, S., Tamura, A., Hayasaka, Y., Katsube, A., Ito, H., Tani, K., Kimura, J.I.,

Chang, Q., Kouchi, Y., Haruta, Y., Yamamoto, K., 2013. An inter-laboratory evaluation of OD-3 zircon for use as a secondary U-Pb dating standard. Island Arc 22 (3), 382–394. http://dx.doi.org/10.1111/iar.12038.

Jackson, S.E., Pearson, N.J., Griffin, W.L., Belousova, E.A., 2004. The application of laser ablation-inductively coupled plasma-mass spectrometry to in situ U-Pb zircon geochronology. Chem. Geol. 211 (1–2), 47–69. http://dx.doi.org/10.1016/j.chemgeo.2004.06.017.

Jaffey, A.H., Flynn, K.F., Glendenin, L.E., Bentley, W.C., Essling, A.M., 1971. Precision measurement of half-lives and specific activities of U-235 and U-238. Phys. Rev. C 4 (5), 1889. http://dx.doi.org/10.1103/PhysRevC.4.1889.

Kaiser, J.F., de Silva, S., Schmitt, A.K., Economos, R., Sunagua, M., 2017. Million-year melt-presence in monotonous intermediate magma fora volcanic-plutonic assemblage in the Central Andes: contrasting histories of crystal-rich and crystal-poor super-sized silicic magmas. Earth Planet. Sci. Lett. 457, 73–86. http://dx.doi.org/10.1016/j.epsl.2016.09.048.

Kennedy, A.K., Wotzlaw, J.F., Schaltegger, U., Crowley, J.L., Schmitz, M., 2014. Eocene zircon reference material for microanalysis of U-Th-Pb isotopes and trace elements. Can. Mineral. 52 (3), 409–421. http://dx.doi.org/10.3749/canmin.52.3.409.

Klotzli, U., Klotzli, E., Gunes, Z., Koslar, J., 2009. Accuracy of laser ablation U-Pb zircon dating: results from a test using five different reference zircons. Geostand. Geoanal. Res. 33 (1), 5–15. http://dx.doi.org/10.1111/j.1751-908X.2009.00921.x.

Košler, J., Wiedenbeck, M., Wirth, R., Hovorka, J., Sylvester, P., Mikova, J., 2005. Chemical and phase composition of particles produced by laser ablation of silicate glass and zircon - implications for elemental fractionation during ICP-MS analysis. J. Anal. At. Spectrom. 20 (5), 402–409. http://dx.doi.org/10.1039/b41629b.

Košler, J., Slama, J., Belousova, E., Corfu, F., Gehrels, G.E., Gerdes, A., Horstwood, M.S.A., Sircombe, K.N., Sylvester, P.J., Tiepolo, M., Whitehouse, M.J., Woodhead, J.D., 2013. U-Pb detrital zircon analysis - results of an inter-laboratory comparison. Geostand. Geoanal. Res. 37 (3), 243–259. http://dx.doi.org/10.1111/j.1751-908X.2013.00245.x.

Kozlov, B., Saint, A., Skroce, A., 2003. Elemental fractionation in the formation of particulates, as observed by simultaneous isotopes measurement using laser ablation ICP-oa-TOFMS. J. Anal. At. Spectrom. 18 (9), 1069–1075.

Kroslakova, I., Günther, D., 2007. Elemental fractionation in laser ablation-inductively coupled plasma-mass spectrometry: evidence for mass load induced matrix effects in the ICP during ablation of a silicate glass. J. Anal. At. Spectrom. 22 (1), 51–62.

Kuhn, H.R., Gunther, D., 2003. Elemental fractionation studies in laser ablation inductively coupled plasma mass spectrometry on laser-induced brass aerosols. Anal. Chem. 75 (4), 747–753. http://dx.doi.org/10.1021/ac0259919.

Kuhn, H.-R., Günther, D., 2004. Laser ablation-ICP-MS: particle size dependent elemental composition studies on filter-collected and online measured aerosols from glass. J. Anal. At. Spectrom. 19 (9), 1158–1164.

Kuhn, H.-R., Guillong, M., Günther, D., 2004. Size-related vaporisation and ionisation of laser-induced glass particles in the inductively coupled plasma. Anal. Bioanal. Chem. 378 (4), 1069–1074.

Kuiper, K.F., Deino, A., Hilgen, F.J., Krijgsman, W., Renne, P.R., Wijbrans, J.R., 2008. Synchronizing rock clocks of earth history. Science 320 (5875), 500–504. http://dx.doi.org/10.1126/science.1154339.

Li, X.H., Long, W.G., Li, Q.L., Liu, Y., Zheng, Y.F., Yang, Y.H., Chamberlain, K.R., Wan, D.F., Guo, C.H., Wang, X.C., Tao, H., 2010. Penglai zircon Megacrysts: a potential new working reference material for microbeam determination of Hf-O isotopes and U-Pb age. Geostand. Geoanal. Res. 34 (2), 117–134. http://dx.doi.org/10.1111/j.1751-908X.2010.00036.x.

Lipman, P.W., McIntosh, W.C., 2008. Eruptive and noneruptive calderas, northeastern San Juan Mountains, Colorado: where did the ignimbrites come from? Geol. Soc. Am. Mem. 120 (7–8), 771–795. http://dx.doi.org/10.1130/b26330.1.

Longerich, H., Günther, D., Jackson, S., 1996. Elemental fractionation in laser ablation inductively coupled plasma mass spectrometry. Fresenius J. Anal. Chem. 355 (5), 538–542.

Lukács, R., Harangi, S., Bachmann, O., Guillong, M., Danisik, M., Buret, Y., von Quadt, A., Dunkl, I., Fodor, L., Sliwinski, J., Soos, I., Szepesi, J., 2015. Zircon geochronology and geochemistry to constrain the youngest eruption events and magma evolution of the mid-Miocene ignimbrite flare-up in the Pannonian Basin, eastern central Europe. Contrib. Mineral. Petrol. 170 (5–6). http://dx.doi.org/10.1007/s00410-015-1206-8.

Marillo-Sialer, E., Woodhead, J., Hergt, J., Greig, A., Guillong, M., Gleadow, A., Evans, N., Paton, C., 2014. The zircon 'matrix effect': evidence for an ablation rate control on the accuracy of U-Pb age determinations by LA-ICP-MS. J. Anal. At. Spectrom. 29 (6), 981–989. http://dx.doi.org/10.1039/c4ja00008k.

Marillo-Sialer, E., Woodhead, J., Hanchar, J.M., Reddy, S.M., Greig, A., Hergt, J., Kohn, B., 2016. An investigation of the laser-induced zircon 'matrix effect' Chem. Geol. 438, 11–24. http://dx.doi.org/10.1016/j.chemgeo.2016:05.014.

Martiny, B.M., Moran-Zenteno, D.J., Solari, L., Loopez-Martinez, M., de Silva, S.L., Flores-Huertas, D., Zuniga-Lagunes, L., Luna-Gonzalez, L., 2013. Caldera formation and progressive batholith construction: geochronological, petrographic and stratigraphic constraints from the Coxcatlan-Tilzapotla area, Sierra Madre del Sur, Mexico. Rev. Mex. Cienc. Geol. 30 (2), 247–267.

Matthews, W.A., Guest, B., 2017. A practical approach for collecting large-n detrital zircon U-Pb data sets by quadrupole LA-ICP-MS. Geostand. Geoanal. Res. 41 (2), 161–180.

Mattinson, J.M., 2005. Zircon U-Pb chemical abrasion ("CA-TIMS") method: combined annealing and multi-step partial dissolution analysis for improved precision and accuracy of zircon ages. Chem. Geol. 220 (1–2), 47–66. http://dx.doi.org/10.1016/j.chemgeo.2005.03.011.

Mattinson, J.M., 2010. Analysis of the relative decay constants of U-235 and U-238 by multi-step CA-TIMS measurements of closed-system natural zircon samples. Chem. Geol. 275 (3–4), 186–198. http://dx.doi.org/10.1016/j.chemgeo.2010.05.007.

Mills, R.D., Coleman, D.S., 2013. Temporal and chemical connections between plutons and ignimbrites from the Mount Princeton magmatic center. Contrib. Mineral. Petrol. 165 (5), 961–980.

Nasdala, L., Wenzel, M., Vavra, G., Irmer, G., Wenzel, T., Kober, B., 2001. Metamictisation of natural zircon: accumulation versus thermal annealing of radioactivity-induced damage. Contrib. Mineral. Petrol. 141 (2), 125–144.

Paces, J.B., Miller, J.D., 1993. Precise U-Pb ages of Duluth complex and related mafic intrusions, northeastern Minnesota - geochronological insights to physical, Petrogenetic, Paleomagnetic, and Tectonomagmatic processes associated with the 1.1 Ga midcontinent rift system. J. Geophys. Res. Solid Earth 98 (B8), 13997–14013. http://dx.doi.org/10.1029/93jb01159.

Pálfy, J., Parrish, R.R., David, K., VÖrÖs, A., 2003. Mid-Triassic integrated U–Pb geochronology and ammonoid biochronology from the Balaton Highland (Hungary). J. Geol. Soc. 160 (2), 271–284.

Paton, C., Woodhead, J.D., Hellstrom, J.C., Hergt, J.M., Greig, A., Maas, R., 2010. Improved laser ablation U-Pb zircon geochronology through robust downhole fractionation correction. Geochem. Geophys. Geosyst. 11. http://dx.doi.org/10.1029/2009gc002618.

Paton, C., Hellstrom, J., Paul, B., Woodhead, J., Hergt, J., 2011. Iolite: freeware for the visualisation and processing of mass spectrometric data. J. Anal. At. Spectrom. 26 (12), 2508–2518. http://dx.doi.org/10.1039/c1ja10172b.

Payacán, I., Gutiérrez, F., Gelman, S.E., Bachmann, O., Parada, M.Á., 2014. Comparing magnetic and magmatic fabrics to constrain the magma flow record in La Gloria pluton, central Chile. J. Struct. Geol. 69, 32–46.

Petrus, J.A., Kamber, B.S., 2012. VizualAge: a novel approach to laser ablation ICP-MS U-Pb geochronology data reduction. Geostand. Geoanal. Res. 36 (3), 247–270. http://dx.doi.org/10.1111/j.1751-908X.2012.00158.x.

Phillips, D., Matchan, E.L., 2013. Ultra-high precision Ar-40/Ar-39 ages for fish canyon tuff and Alder Creek rhyolite sanidine: new dating standards required? Geochim. Cosmochim. Acta 121, 229–239. http://dx.doi.org/10.1016/j.gca.2013.07.003.

von Quadt, A., Gallhofer, D., Guillong, M., Peytcheva, I., Waelle, M., Sakata, S., 2014. U-Pb dating of CA/non-CA treated zircons obtained by LA-ICP-MS and CA-TIMS techniques: impact for their geological interpretation. J. Anal. At. Spectrom. 29 (9), 1618–1629. http://dx.doi.org/10.1039/c4ja00102h.

von Quadt, A., Wotzlaw, J.F., Buret, Y., Large, S.J.E., Peytcheva, I., Trinquier, A., 2016. High-precision zircon U/Pb geochronology by ID-TIMS using new 10(13) ohm resistors. J. Anal. At. Spectrom. 31 (3), 658–665. http://dx.doi.org/10.1039/c5ja00457h.

Reid, M.R., Vazquez, J.A., 2017. Fitful and protracted magma assembly leading to a Giant eruption, Youngest Toba Tuff, Indonesia. Geochem. Geophys. Geosyst. 18 (1), 156–177.

Reid, M.R., Coath, C.D., Harrison, T.M., McKeegan, K.D., 1997. Prolonged residence times for the youngest rhyolites associated with Long Valley Caldera: Th-230-U-238 ion microprobe dating of young zircons. Earth Planet. Sci. Lett. 150 (1–2), 27–39. http://dx.doi.org/10.1016/S0012-821x(97)00077-0.

Renne, P.R., Swisher, C.C., Deino, A.L., Karner, D.B., Owens, T.L., DePaolo, D.J., 1998. Intercalibration of standards, absolute ages and uncertainties in Ar-40/Ar-39 dating (vol 145, pg 117, 1998). Chem. Geol. 149 (3–4) (259-259). http://dx.doi.org/10.1016/S0009-2541(98)00047-3.

Renne, P.R., Mundil, R., Balco, G., Min, K.W., Ludwig, K.R., 2010. Joint determination of K-40 decay constants and Ar-40*/K-40 for the Fish Canyon sanidine standard, and improved accuracy for Ar-40/Ar-39 geochronology. Geochim. Cosmochim. Acta 74 (18), 5349–5367. http://dx.doi.org/10.1016/j.gca.2010.06.017.

Rivera, T.A., Storey, M., Zeeden, C., Hilgen, F.J., Kuiper, K., 2011. A refined astronomically calibrated Ar-40/Ar-39 age for Fish Canyon sanidine. Earth Planet. Sci. Lett. 311 (3–4), 420–426. http://dx.doi.org/10.1016/j.epsl.2011.09.017.

Rubatto, D., Hermann, J., 2007. Experimental zircon/melt and zircon/garnet trace element partitioning and implications for the geochronology of crustal rocks. Chem. Geol. 241 (1–2), 38–61. http://dx.doi.org/10.1016/j.chemgeo.2007.01.027.

Sakata, S., Hattori, K., Iwano, H., Yokoyama, T.D., Danhara, T., Hirata, T., 2014. Determination of U-Pb ages for young zircons using laser ablation-ICP-mass spectrometry coupled with an ion detection attenuator device. Geostand. Geoanal. Res. 38 (4), 409–420. http://dx.doi.org/10.1111/j.1751-908X.2014.00320.x.

Sakata, S., Hirakawa, S., Iwano, H., Danhara, T., Guillong, M., Hirata, T., 2017. A new approach for constraining the magnitude of initial disequilibrium in Quaternary zircons by coupled uranium and thorium decay series dating. Quat. Geochronol. 38, 1–12. http://dx.doi.org/10.1016/j.quageo.2016.11.002.

Samperton, K.M., Schoene, B., Cottle, J.M., Keller, C.B., Crowley, J.L., Schmitz, M.D., 2015. Magma emplacement, differentiation and cooling in the middle crust: integrated zircon geochronological-geochemical constraints from the Bergell Intrusion, Central Alps. Chem. Geol. 417, 322–340. http://dx.doi.org/10.1016/j.chemgeo.2015.10.024.

Samperton, K.M., Bell, E.A., Barboni, M., Keller, C.B., Schoene, B., 2017. Zircon Age-temperature-Compositional Spectra in Plutonic Rocks.

Schaen, A.J., Cottle, J.M., Singer, B.S., Keller, C.B., Garibaldi, N., Schoene, B., 2017. Complementary crystal accumulation and rhyolite melt segregation in a late Miocene Andean pluton. Geology 45 (9), 835–838.

Schaltegger, U., Schmitt, A.K., Horstwood, M.S.A., 2015. U-Th-Pb zircon geochronology by ID-TIMS, SIMS, and laser ablation ICP-MS: recipes, interpretations, and opportunities. Chem. Geol. 402, 89–110. http://dx.doi.org/10.1016/j.chemgeo.2015.02.028.

Schärer, U., 1984. The effect of initial 230Th disequilibrium on young UPb ages: the Makalu case, Himalaya. Earth Planet. Sci. Lett. 67 (2), 191–204. http://dx.doi.org/10.1016/0012-821X(84)90114-6.

Schmitt, A.K., Lindsay, J.M., de Silva, S., Trumbull, R.B., 2003. U-Pb zircon chronostratigraphy of early-Pliocene ignimbrites from La Pacana, north Chile: implications for the formation of stratified magma chambers. J. Volcanol. Geotherm. Res. 120

(1–2), 43–53. (doi:Pii S0377–0273(02)00359–1). http://dx.doi.org/10.1016/S0377-0273(02)00359-1.

Schoene, B., Schaltegger, U., Brack, P., Latkoczy, C., Stracke, A., Gunther, D., 2012. Rates of magma differentiation and emplacement in a ballooning pluton recorded by U-Pb TIMS-TEA, Adamello batholith, Italy. Earth Planet. Sci. Lett. 355, 162–173. http://dx.doi.org/10.1016/j.epsl.2012.08.019.

Silver, L.T., Deutsch, S., 1963. Uranium-lead isotopic variations in zircons: a case study. J. Geol. 721–758.

Simonetti, A., Heaman, L.M., Hartlaub, R.P., Creaser, R.A., MacHattie, T.G., Böhm, C., 2005. U–Pb zircon dating by laser ablation-MC-ICP-MS using a new multiple ion counting Faraday collector array. J. Anal. At. Spectrom. 20 (8), 677–686.

Sláma, J., Kosler, J., Condon, D.J., Crowley, J.L., Gerdes, A., Hanchar, J.M., Horstwood, M.S.A., Morris, G.A., Nasdala, L., Norberg, N., Schaltegger, U., Schoene, B., Tubrett, M.N., Whitehouse, M.J., 2008. Plesovice zircon - a new natural reference material for U-Pb and Hf isotopic microanalysis. Chem. Geol. 249 (1–2), 1–35. http://dx.doi.org/10.1016/j.chemgeo.2007.11.005.

Solari, L.A., Ortega-Obregon, C., Bernal, J.P., 2015. U-Pb zircon geochronology by LAICPMS combined with thermal annealing: achievements in precision and accuracy on dating standard and unknown samples. Chem. Geol. 414, 109–123. http://dx.doi.org/10.1016/j.chemgeo.2015.09.008.

Steiger, R.H., Jäger, E., 1977. Subcommission on geochronology: convention on the use of decay constants in geo-and cosmochronology. Earth Planet. Sci. Lett. 36 (3), 359–362.

Stern, R.A., Bodorkos, S., Kamo, S.L., Hickman, A.H., Corfu, F., 2009. Measurement of SIMS instrumental mass fractionation of Pb isotopes during zircon dating. Geostand. Geoanal. Res. 33 (2), 145–168. http://dx.doi.org/10.1111/j.1751-908X.2009.00023.x.

Storm, S., Shane, P., Schmitt, A.K., Lindsay, J.M., 2012. Decoupled crystallization and eruption histories of the rhyolite magmatic system at Tarawera volcano revealed by zircon ages and growth rates. Contrib. Mineral. Petrol. 163 (3), 505–519. http://dx.doi.org/10.1007/s00410-011-0682-8.

Tilton, G.R., 1956. The interpretation of lead-age discrepancies by acid-washing experiments. EOS Trans. Am. Geophys. Union 37 (2), 224–230.

Vazquez, J.A., Reid, M.R., 2004. Probing the accumulation history of the voluminous Toba magma. Science 305 (5686), 991–994. http://dx.doi.org/10.1126/science.1096994.

Watts, K.E., Coble, M.A., Vazquez, J.A., Henry, C.D., Colgan, J.P., John, D.A., 2016. Chemical abrasion-SIMS (CA-SIMS) U-Pb dating of zircon from the late Eocene Caetano caldera, Nevada. Chem. Geol. 439, 139–151. http://dx.doi.org/10.1016/j.chemgeo.2016.06.013.

Westerhold, T., Rohl, U., Laskar, J., 2012. Time scale controversy: accurate orbital calibration of the early Paleogene. Geochem. Geophys. Geosyst. 13. http://dx.doi.org/10.1029/2012gc004096.

Wiedenbeck, M., Alle, P., Corfu, F., Griffin, W.L., Meier, M., Oberli, F., Vonquadt, A., Roddick, J.C., Speigel, W., 1995. 3 natural zircon standards for U-Th-Pb, Lu-Hf, trace-element and ree analyses. Geostand. Newslett. 19 (1), 1–23. http://dx.doi.org/10.1111/j.1751-908X.1995.tb00147.x.

Wotzlaw, J.F., Schaltegger, U., Frick, D.A., Dungan, M.A., Gerdes, A., Gunther, D., 2013. Tracking the evolution of large-volume silicic magma reservoirs from assembly to supereruption. Geology 41 (8), 867–870. http://dx.doi.org/10.1130/G34366.1.

Zimmerer, M.J., McIntosh, W.C., 2012. An investigation of caldera-forming magma chambers using the timing of ignimbrite eruptions and pluton emplacement at the Mt. Aetna caldera complex. J. Volcanol. Geotherm. Res. 245, 128–148. http://dx.doi.org/10.1016/j.jvolgeores.2012.08.007.